

An Empirical Study on Knowledge Transfer under Domain and Label Shifts in 3D LiDAR Point Clouds

Subeen Lee^{1*} Siyeong Lee² Namil Kim² Jaesik Choi^{1†}

¹KAIST ²NAVERLABS

{sbrblee7, jaesik.choi}@kaist.ac.kr, {siyeong.lee, namil.kim}@naverlabs.com

Abstract

For 3D perception systems to be practical in real-world applications—from autonomous driving to embodied AI—models must adapt to continuously evolving object definitions and sensor domains. Yet, research on continual and transfer learning in 3D point cloud perception remains underexplored compared to 2D vision—particularly under simultaneous domain and label shifts. To address this gap, we propose the **RObust Autonomous driving under Dataset shifts (ROAD)** benchmark, a comprehensive evaluation suite for LiDAR-based object classification that explicitly accounts for domain shifts as well as three key forms of label evolution: class split, class expansion, and class insertion. Using large-scale datasets (Waymo, NuScenes, Argoverse2), we evaluate zero-shot transfer, linear probe, and CL, and analyze the impact of backbone architectures, training objectives, and CL methods. Our findings reveal limitations of existing approaches under realistic shifts and establish strong baselines for future research in robust 3D perception.

1. Introduction

Knowledge is not static; it continuously expands and evolves, leading to increasingly complex and large-scale problem formulations and models in the real world. Amid these dynamics, researchers seek models that can flexibly adapt to such changes in knowledge (learning plasticity), retain essential prior knowledge (memory stability), and generalize well across diverse data distributions (generalizability) [61]. In deep learning, since creating a new model every time new knowledge is acquired is costly, methods such as zero-shot learning [63], few-shot learning [64], domain adaptation [62], and continual learning [61] have been actively explored to enable efficient knowledge transfer.

Despite these advances, most studies assume simplified problem settings that overlook real-world complexity. In continual learning (CL), for example, tasks are typically treated independently as class-, domain-, or task-incremental learning [61], often under strong assumptions such as disjoint class sets across sessions [11, 19, 46]. Recent works have begun to relax these constraints by introducing more realistic CL scenarios [1, 3, 5, 27, 30, 52, 70], but these efforts remain primarily confined to 2D image benchmarks. In contrast, 3D point cloud domains—especially LiDAR-based perception in autonomous driving—are still underexplored, despite common and nuanced shifts from sensor differences, environmental variation, and geographic diversity [18, 65, 73]. Label inconsistencies are also common, driven by variations in taxonomies, annotation protocols, and label granularity [6, 21, 56]. While domain adaptation has been extensively studied under the assumption of a fixed label space [8, 18, 73], such approaches fail to address scenarios where models must expand to new label taxonomies. They also overlook the challenges posed by simultaneous domain and label shifts. These complex, intertwined shifts hinder model transfer, complicate continual adaptation, and underscore the need to assess generalization under more realistic and demanding conditions.

To address these gaps, this study proposes a benchmark framework named **ROAD** that systematically characterizes dataset shifts in 3D perception tasks—not only in terms of domain shift, but also through several forms of label shift—Coarse-to-Fine-Grained Label Expansion (**Class Split**), (2) Intra-Class Knowledge Expansion (**Class Expansion**), and (3) New Class Introduction (**Class Insertion**). We assess how flexibly a model can transfer and adapt its learned knowledge, using different tasks—zero-shot transfer, linear probe, and continual learning. Furthermore, we investigate how well commonly adopted design choices—such as model architectures, base training (or pretraining) strategies, and continual learning approaches—perform under these more realistic and challeng-

*Work done during intern at NAVER LABS.

†Corresponding author.

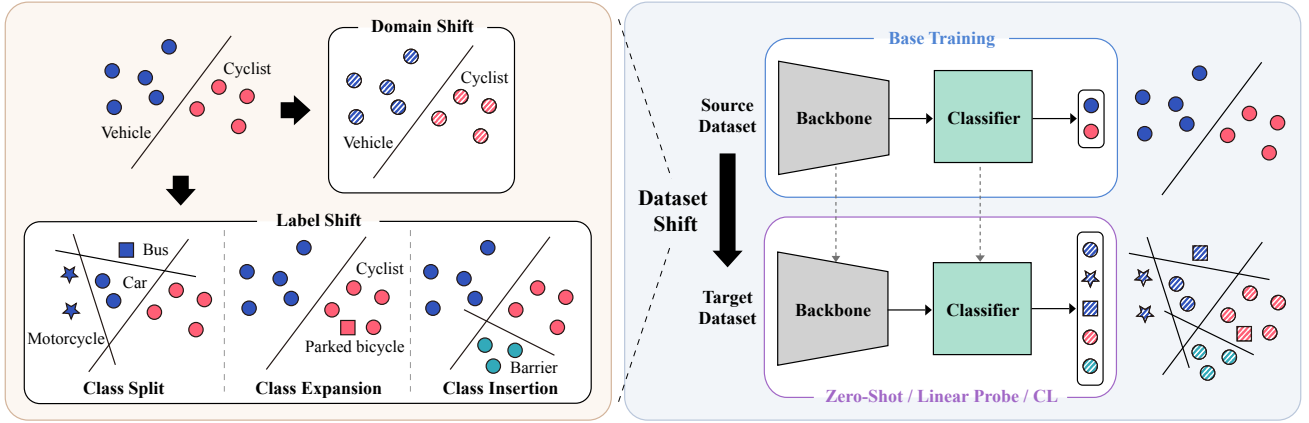


Figure 1. Overview of our benchmarking framework.

ing shift scenarios, instantiated by Waymo Open Dataset [56], NuScenes Dataset [6], and Argoverse2 Dataset [67].

Prior research in 3D perception has predominantly focused on 3D object detection—combining object classification and localization—across various sensor modalities such as RGB, LiDAR, or their fusion. To isolate and better understand the effects of complex shifts in 3D perception, we simplify the problem to a LiDAR-only object classification task. This choice also enables a focused analysis of a critical failure mode in object detection: objects that are detected but misclassified (e.g., a pedestrian predicted as a vehicle), which can lead to potentially dangerous outcomes in downstream detection systems [49].

The contributions of our work are as follows:

- **A Realistic Benchmark for Knowledge Transfer in 3D LiDAR Point Clouds:** We introduce a benchmark that jointly considers domain and label shifts using large-scale datasets (Waymo-to-NuScenes, Waymo-to-Argoverse2). To our knowledge, this is the first to explore knowledge transfer on the challenging Waymo-to-Argoverse2 setting, offering a faithful testbed for real-world deployment.
- **Unified Evaluation Protocol Across Paradigms:** Our protocol spans zero-shot transfer, linear probe, and continual learning, capturing adaptability across both short- and long-term knowledge evolution—largely overlooked in prior studies in 3D point clouds.
- **Systematic Analysis of Design Choices:** We provide the first comparison of how backbones, training objectives, and CL methods affect generalization in 3D knowledge transfer, establishing strong baselines and offering insights for future model design.

2. ROAD: A Benchmark for Robust Autonomous Driving under Dataset Shifts

Fig. 1 illustrates the overall framework of our study. We define four types of dataset shift in autonomous driving perception, focusing on scenarios where a pre-trained model must adapt to evolving environments. Within this framework, we analyze the effects of backbone architecture, base training strategy, and continual learning methods.

2.1. Dataset Shifts

Let \mathbb{D} denote a data distribution and \mathcal{C} a set of class labels. Consider a source dataset $(\mathcal{X}_S, \mathcal{Y}_S)$ with $\mathcal{X}_S \sim \mathbb{D}_S$, $\mathcal{Y}_S \subseteq \mathcal{C}_S$, and a target dataset $(\mathcal{X}_T, \mathcal{Y}_T)$ with $\mathcal{X}_T \sim \mathbb{D}_T$, $\mathcal{Y}_T \subseteq \mathcal{C}_T$. We define *dataset shifts* as cases where $\mathbb{D}_S \neq \mathbb{D}_T$ and/or $\mathcal{C}_S \neq \mathcal{C}_T$. A *domain shift* arises when the data distributions differ [2, 35], i.e., $\mathbb{D}_S \neq \mathbb{D}_T$, which can result from factors such as heterogeneous sensors, shapes of LiDAR beams, size distribution of bounding boxes, or varying environmental conditions [18, 66, 73]. A *label shift* arises when the label sets differ, $\mathcal{C}_S \neq \mathcal{C}_T$. We further categorize label shift into three types: *class split*, *class expansion*, and *class insertion*. In Tab. 1 and Tab. 2, we summarize potential causes of dataset shifts and examples of label shifts in the Waymo-to-NuScenes and Waymo-to-Argoverse2 settings, respectively, where “A-to-B” denotes transfer from source dataset A to target dataset B.

Class Split (\leftrightarrow Merge) Label definitions in autonomous driving often evolve, either by splitting coarse categories into finer subcategories (*class split*) or by merging fine-grained ones into broader categories (*class merge*). While such dynamics resemble hierarchical classification, most existing methods assume a fixed label hierarchy during base training [24], which is unrealistic in continually evolving scenarios. This uncertainty, however, poses a critical challenge: models trained on coarse labels must not only clas-

| LiDAR Sensor | | Site | Vertical FOV | # Beams | Average (l, w, h) | Average # Points per Object |
|-----------------|----------------------|----------------------------------------------------------------|--------------|---------|---------------------|-----------------------------|
| Waymo [56] | Laser Bear Honeycomb | Phoenix, San Francisco, Mountain View | 95° | 64 | (3.5, 1.6, 1.8)m | 310. |
| NuScenes [6] | Velodyne HDL-32E | Boston, Singapore | 40° | 32 | (4.9, 2.1, 2.0)m | 75. |
| Argoverse2 [67] | Two Velodyne VLP-32C | Austin, Detroit, Miami, Pittsburgh, Palo Alto, Washington, D.C | 40° | 64 | (4.3, 1.8, 1.9)m | 177. |

Table 1. Descriptions of Waymo, NuScenes, and Argoverse2 datasets. (l, w, h) refers to the size of a bounding box.

| Type of Shift | Source | Target | | |
|-------------------------|------------|--------------------------------------------------------------|--------------------------------------------------------------------------------------------------------------------------------------------------|---|
| | Waymo | NuScenes | Argoverse2 | |
| Class Split | vehicle | car, truck, bus, motorcycle construction_vehicle, trailer | regular_vehicle, large_vehicle, bus box_truck, truck, motorcycle truck_cab, motorcyclist, school_bus vehicular_trailer, articulated_bus | |
| | pedestrian | - | pedestrian, wheeled_rider | |
| Class Expansion | cyclist | bicycle | | - |
| Class Split + Expansion | pedestrian | - | stroller | |
| Class Insertion | - | barrier, traffic_cone | bollard, sign, construction_barrel stop_sign, bicycle, wheeled_device mobile_pedestrian_crossing_sign | |
| Maintained | pedestrian | pedestrian | | - |
| | cyclist | - | cyclist | |

Table 2. Label shifts between Waymo (source) and NuScenes/Argoverse2 (target).

sify the current categories but also learn representations expressive enough to capture latent fine-grained distinctions that may later split. To evaluate this capability, we measure performance on split classes $\mathcal{C}_{split} \subseteq \mathcal{C}_T$, following [39].

Class Expansion (\leftrightarrow Reduction) Even when a similar class label set is used for source and target datasets, the definition of classes may vary. For example, in Waymo, riderless bicycles are ignored and only the objects with riders labeled as `cyclist`, whereas in NuScenes, all bicycles—regardless of rider presence—are labeled as `bicycle`. As a result, the bicycle class in NuScenes encompasses a broader range of instances, including cyclists, parked bicycles, and bicycles lying on the ground. When adapting models from Waymo to NuScenes, this type of semantic expansion is often overlooked, with prior work typically treating the two label definitions as equivalent [38]. However, such differences in labeling semantics can pose significant challenges to the effective transfer of knowledge. For instance, under our Waymo-to-NuScenes zero-shot transfer setting, NuScenes bicycle instances without riders exhibit significantly lower prediction accuracy (**62.3%**) compared to those with riders (**100%**) (PointNet++ backbone,

cross-entropy loss as a base objective).

Class Insertion (\leftrightarrow Deletion) The emergence of new classes is a common scenario in real-world applications, occurring when new concepts are introduced or previously unclassified objects need to be identified. For example, electric scooters, which have recently become a prevalent form of individual transportation, may be introduced as a new category in autonomous driving datasets as additional data is collected over time. Such class insertion is usually studied under class-incremental learning (CIL), but in practice, it often coincides with domain shift, since the new data is gathered in different environments.

2.2. Knowledge Transfer Tasks

To analyze dataset shifts in terms of model generalizability, we consider three knowledge transfer tasks—**zero-shot transfer**, **linear probe**, and **continual learning**—which progressively require greater flexibility in utilizing the model’s representation space. Given a base model f_S trained on $(\mathcal{X}_S, \mathcal{Y}_S)$ with loss \mathcal{L}_S (the base objective), applying it directly to \mathcal{X}_T without further training corresponds to **zero-shot transfer**. When the label domains

differ ($\mathcal{Y}_S \neq \mathcal{Y}_T$), we apply appropriate mappings: split classes are mapped to their unsplit superclass, expanded classes to their original class, and inserted classes are excluded. If the backbone is frozen but a last linear layer of the classifier is fine-tuned on $(\mathcal{X}_T, \mathcal{Y}_T)$ with loss \mathcal{L}_T , we call this **linear probe (LP)**. If the entire model is fine-tuned with an additional regularization term— $\mathcal{L}_T + \lambda \mathcal{L}_{reg}$, where λ controls the strength—to mitigate forgetting, we call this **continual learning (CL)**. For \mathcal{L}_T , we use cross-entropy loss for target classes.

Scope We restrict our study to classification tasks without leveraging pretrained models and external datasets beyond the given source and target. Each dataset is assumed to be fully accessible only during its respective training session, i.e., training is conducted offline, without access to the other session’s data. Semantic relationships (mappings) between class labels across sessions are not available during training and are only revealed at evaluation.

Evaluation Metrics We utilize class-averaged accuracy $R_{dataset, model}$ for each dataset and model. For the CL setting, we additionally use backward transfer (**BWT**) and source-target-averaged accuracy (**ACC**), formulated as follows [33]:

$$\begin{aligned} \text{BWT} &= R_{S, f_T} - R_{S, f_S} \\ \text{ACC} &= \frac{1}{2}(R_{S, f_T} + R_{T, f_T}) \end{aligned} \quad (1)$$

2.3. Design Choices

We analyze how different design choices affect performance across the knowledge transfer tasks under the dataset shifts introduced above.

Backbone Architectures Similar to [18], who studied the impact of architectural components of 3D object detectors on domain generalizability, we examine the role of backbone architecture in classification. We assume the classifier consists of a feature-extraction backbone and simple MLP classifier layers (we chose a four-layer linear classifier head). For the backbone, we adopt two widely used point-based models: PointNet++ [44] and Point Transformer [75].

Base Objectives Since the training objective influences model generalizability [21, 23, 50], we compare different objectives for \mathcal{L}_S to examine how they shape the base model’s representations and, in turn, affect performance. We evaluated eight objectives: **cross-entropy (CE)**, **dot regression (DR)** [71], **adversarial reciprocal points learning (ARPL)** [12], **supervised contrastive learning (Sup-Con)** [25], **InfoNCE (NCE)** [13], **VICReg (VR)** [4], **NCE + CE (NCECE)**, and **VICReg + CE (VRCE)**. The first four rely on class-label supervision. SupCon, NCE, and VR models are first trained in a (self-)supervised manner, followed by last-layer fine-tuning with cross-entropy loss for source classes (two-phase). The last two combine

both objectives jointly (single-phase). We refer to the four self-supervised loss-assisted models (NCE, NCECE, VR, VRCE) as **SSL models**.

Continual Learning Approaches Under the label shifts defined above, the source and target class sets are not necessarily disjoint. However, most prior works on CL for 3D point clouds have focused on CIL, typically assuming disjoint class sets across sessions [17, 47, 48, 57, 72]. Yet, when classes across domains are semantically related—for example, a coarse class in the source split into finer classes in the target—it is not necessary to force the model to treat them as entirely separate. In such cases, the model can map semantically dependent classes to the same category—as opposed to the mapping in zero-shot transfer—while introducing new classifier outputs only for inserted classes.

To explore this, we compare two setups:

- **Extension Head**: a conventional CIL approach, where the classifier head is expanded whenever a new target dataset is introduced. e.g., In Waymo-to-NuScenes, the classifier head output dimension is increased from 3 to 13 (3+10) in our setting.
- **Inclusive Head**: an alternative approach, where the classifier head maintains a unified label space across sessions. e.g., In Waymo-to-NuScenes, the classifier head output dimension is increased from 3 to 10 in our setting.

In the **Extension Head** setup, we adopt **Learning without Forgetting (LwF)** [32]. This knowledge distillation method preserves performance on previously learned classes by enforcing the source head logits of target samples to remain consistent. In contrast, the **Inclusive Head** setup employs **Elastic Weight Consolidation (EWC)** [26], which regularizes updates to parameters critical for past tasks to mitigate catastrophic forgetting.

While existing CL methods for point clouds often rely on rehearsal-based strategies [48, 72] or make strong architecture-specific assumptions [17, 47], we adopt methods that are architecture-agnostic and do not require access to old data, aiming for a more general-purpose benchmark.

3. Experimental Results

3.1. Setup

Datasets Preparation We used the Waymo Open Dataset [56] as the source and NuScenes [6] and Argoverse2 [67] as targets. We denote Waymo-to-NuScenes as **W→N** and Waymo-to-Argoverse2 as **W→A** for brevity. All three are large-scale autonomous driving datasets but differ in domain and label taxonomies. Following OpenPCDet [58] and official annotations [6, 56, 67], we summarize selected classes and types of label shifts in Tab. 2. Waymo defines coarse categories (vehicle, pedestrian, cyclist), while NuScenes and Argoverse2 introduce finer-grained ve-

| Waymo | | | | W→N (Zero-Shot) | | | W→A (Zero-Shot) | | | | |
|-------------------|--------|-------------|-------------|-----------------|-------------|-------------|-----------------|-------------|-------------|-------------|------------|
| | Veh. | Ped. | Cyc. | Veh.S. | Ped.M. | Cyc.E. | Veh.S. | Ped.S. | Ped.SE. | Cyc.M. | |
| PointNet++ | CE | 98.5 | 99.4 | 88.8 | 91.7 | 98.2 | 70.2 | 77.1 | 97.1 | 91.6 | 1.6 |
| | DR | 99.7 | 96.8 | 96.8 | 99.7 | 85.9 | 17.5 | 87.3 | 79.0 | 69.0 | 1.9 |
| | ARPL | 99.3 | 96.9 | 89.1 | 95.7 | 85.8 | 64.9 | 81.9 | 87.0 | 38.0 | 5.9 |
| | SupCon | 98.4 | 96.1 | 92.7 | 93.7 | 83.4 | 49.1 | 79.7 | 86.8 | 77.5 | 4.4 |
| | NCE | 99.3 | 93.2 | 86.5 | 95.1 | 61.4 | 52.6 | 77.4 | 91.3 | 19.7 | 4.4 |
| | NCECE | 99.5 | 98.8 | 95.3 | 96.3 | 95.3 | 59.7 | 82.7 | 95.4 | 95.8 | 1.6 |
| | VR | 96.6 | 85.0 | 80.7 | 97.8 | 20.2 | 17.5 | 59.3 | 92.9 | 80.3 | 2.8 |
| | VRCE | 99.7 | 97.0 | 94.0 | 96.5 | 82.1 | 52.6 | 85.6 | 90.1 | 85.9 | 5.0 |
| Point Transformer | CE | 99.4 | 98.1 | 92.1 | 93.5 | 96.4 | 54.4 | 85.1 | 93.6 | 95.8 | 1.2 |
| | DR | 99.5 | 91.9 | 83.8 | 93.5 | 89.9 | 24.6 | 90.5 | 67.5 | 90.1 | 5.9 |
| | ARPL | 98.7 | 97.1 | 89.8 | 92.2 | 92.9 | 59.7 | 86.3 | 84.1 | 97.2 | 2.5 |
| | SupCon | 98.9 | 97.1 | 91.3 | 91.6 | 90.4 | 68.4 | 88.0 | 80.5 | 95.8 | 1.2 |
| | NCE | 98.4 | 88.0 | 89.4 | 89.6 | 82.5 | 63.2 | 87.4 | 60.4 | 69.0 | 0.6 |
| | NCECE | 99.0 | 98.6 | 91.0 | 89.4 | 92.8 | 50.9 | 84.7 | 86.2 | 85.9 | 1.2 |
| | VR | 98.2 | 86.7 | 79.0 | 87.0 | 74.8 | 75.4 | 92.2 | 51.1 | 74.6 | 0.9 |
| | VRCE | 98.9 | 99.1 | 87.6 | 91.3 | 95.9 | 79.0 | 85.8 | 99.1 | 95.8 | 0.6 |

Table 3. Accuracies(%) of base models on the validation datasets of Waymo, NuScenes, and Argoverse2. Veh., Ped., and Cyc. denote the vehicle, pedestrian, and cyclist classes, respectively. In the zero-shot transfer setting, class names are followed by the type of label shift: S = split, E = expansion, SE = split + expansion, M = maintained.

hicle and/or pedestrian subclasses and additional expanded or inserted classes.

We extracted object-level samples from 3D bounding boxes. For model input, we used only the 3D coordinates (xyz) and intensity of points, with xyz coordinates normalized to $[-1, 1]$ within each bounding box, and objects with fewer than 64 points are discarded. This yielded 1.04M/0.25M train/val samples in Waymo, 0.12M/0.02M in NuScenes, and 1.93M/0.39M in Argoverse2. For Waymo, we additionally applied pseudo line downsampling [66] from 64 to 32 beams. Further experimental details are explained in Sec. A.

Base & LP Model Training We applied standard augmentations (flip, rotation, scaling, sampling, shuffling) and balanced resampling. SSL models used two augmented views per sample. Optimization used Adam ($lr=0.001$, batch=128), except for Point Transformer ARPL ($lr=10^{-5}$ due to convergence issues). Training lasted 10 epochs for base models and 10 (NuScenes) or 1 (Argoverse2) epochs for LP models. For NCECE and VRCE, loss coefficients were 0.1 (SSL) and 1.0 (CE).

CL Model Training We experimented with different λ values: [0.25, 0.5, 0.75, 1.0, 1.25, 1.5] for LwF and [0.0005, 0.001, 0.005, 0.01, 0.05, 0.1] for EWC. Base models were fine-tuned for 20 (NuScenes) or 2 (Argoverse2) epochs. The importance weights for EWC were estimated via batched empirical Fisher [10, 77], calculated by each class in the

source dataset and then averaged. As baselines, **FT models** were obtained by fine-tuning without regularization.

Evaluation For target evaluation in zero-shot transfer and source evaluation in CL, class mappings follow Tab. 2. In zero-shot transfer, e.g., a NuScenes bus predicted as vehicle is correct. In W→N CL, a Waymo vehicle is correct if classified into any of [car, truck, bus, motorcycle, construction_vehicle, trailer].

3.2. Results

Accuracies are reported in Tab. 3 (zero-shot transfer), Tabs. 4 and 5 (LP) and Tabs. 11 to 14 (CL). Cells are color-coded for clarity, with brighter colors indicating higher accuracy, and bold values denoting the best performance in each backbone.

3.2.1. Summary

NuScenes vs. Argoverse2: Overall, W→A involves stronger dataset shifts than W→N, making transfer harder.

Label shift: Zero-shot transfer handles class split cases well at the coarse level, but LP and CL struggle with fine-grained classification. Class split is hardest in LP, while class expansion shows larger model-dependent variation. **Backbone:** No backbone architecture consistently outperforms; performance depends on its pairing with the base objective. **Base objective:** SSL models excel in LP but not in CL, where DR models perform worst under LwF. **CL approach:** Among

CL methods, LwF effectively mitigates forgetting, whereas EWC often fails with stability issues.

| | W→N LP | Veh.S. | Ped.M. | Cyc.E. | Insert. |
|-------------------|--------|--------|--------|--------|---------|
| PointNet++ | CE | 21.4 | 88.0 | 54.4 | 38.5 |
| | DR | 23.4 | 82.4 | 93.0 | 40.1 |
| | ARPL | 20.7 | 90.3 | 73.7 | 26.3 |
| | SupCon | 19.9 | 84.0 | 38.6 | 18.2 |
| | NCE | 40.4 | 80.3 | 40.4 | 71.5 |
| | NCECE | 44.6 | 82.6 | 84.2 | 70.7 |
| | VR | 32.4 | 72.3 | 61.4 | 72.5 |
| | VRCE | 32.3 | 52.5 | 80.7 | 57.1 |
| Point Transformer | CE | 19.7 | 89.1 | 86.0 | 16.8 |
| | DR | 24.2 | 90.0 | 82.5 | 20.8 |
| | ARPL | 16.0 | 83.7 | 91.2 | 15.6 |
| | SupCon | 21.0 | 80.3 | 98.3 | 17.9 |
| | NCE | 44.4 | 77.0 | 66.7 | 57.7 |
| | NCECE | 44.2 | 79.1 | 86.0 | 50.8 |
| | VR | 34.6 | 70.4 | 63.2 | 48.4 |
| | VRCE | 33.9 | 78.9 | 80.7 | 45.7 |

Table 4. Accuracies(%) of linear probes on the NuScenes dataset.

3.2.2. Zero-Shot Transfer & Linear Probe

Zero-shot transfer yielded consistently low cyclist accuracy across datasets, backbones, and objectives. Even in W→A, where the class definition of cyclist is preserved, accuracy remained poor, likely due to overfitting on this minor class and amplifying domain shift. For vehicle and pedestrian classes, the models performed relatively better, suggesting partial generalizability, but no backbone-objective pair was consistently superior.

In LP, however, **SSL models outperform supervised ones in both vehicle class split and class insertion cases**. This indicates that self-supervised objectives shaped feature spaces more effectively for fine-grained and novel class recognition. In W→A, Point Transformer further highlights SSL benefits for pedestrian and cyclist classes. As shown in Fig. 8, t-SNE embeddings confirmed that SSL models produce more disentangled feature spaces, particularly for split vehicle subclasses and inserted classes.

3.2.3. Continual Learning

In Fig. 2, we show the performance of CL models varying λ values, highlighting the trade-off between source and target accuracy. Fig. 3 presents the best-performing models for each backbone-objective pair.

LwF consistently outperforms EWC. Most LwF models lie above FT on the Pareto front, while EWC performed on par with or worse than FT, highlighting its limited ability to retain source knowledge and vulnerability to catastrophic forgetting.

| | W→A LP | Veh.S. | Ped.S. | Ped.SE. | Cyc.M | Insert. |
|-------------------|--------|--------|--------|---------|-------|---------|
| PointNet++ | CE | 9.4 | 39.5 | 42.2 | 24.6 | 23.0 |
| | DR | 8.8 | 35.6 | 42.2 | 10.9 | 20.8 |
| | ARPL | 10.3 | 25.5 | 2.8 | 24.9 | 23.6 |
| | SupCon | 9.0 | 12.7 | 21.1 | 5.0 | 23.7 |
| Point Transformer | NCE | 25.1 | 48.0 | 83.1 | 48.3 | 36.5 |
| | NCECE | 27.1 | 50.3 | 80.3 | 49.5 | 44.4 |
| | VR | 14.7 | 24.1 | 32.4 | 48.3 | 35.9 |
| | VRCE | 15.9 | 55.9 | 52.1 | 19.3 | 32.1 |
| Point Transformer | CE | 9.8 | 34.2 | 0.0 | 5.9 | 12.6 |
| | DR | 9.4 | 31.1 | 0.0 | 15.9 | 21.7 |
| | ARPL | 8.4 | 0.0 | 1.4 | 0.0 | 24.4 |
| | SupCon | 9.1 | 0.0 | 9.9 | 0.0 | 19.4 |
| Point Transformer | NCE | 26.4 | 18.5 | 35.2 | 40.5 | 40.0 |
| | NCECE | 27.3 | 22.4 | 25.4 | 31.8 | 39.9 |
| | VR | 15.2 | 18.4 | 38.0 | 57.9 | 28.4 |
| | VRCE | 14.4 | 21.5 | 36.6 | 39.2 | 32.3 |

Table 5. Accuracies(%) of linear probes on the Argoverse2 dataset.

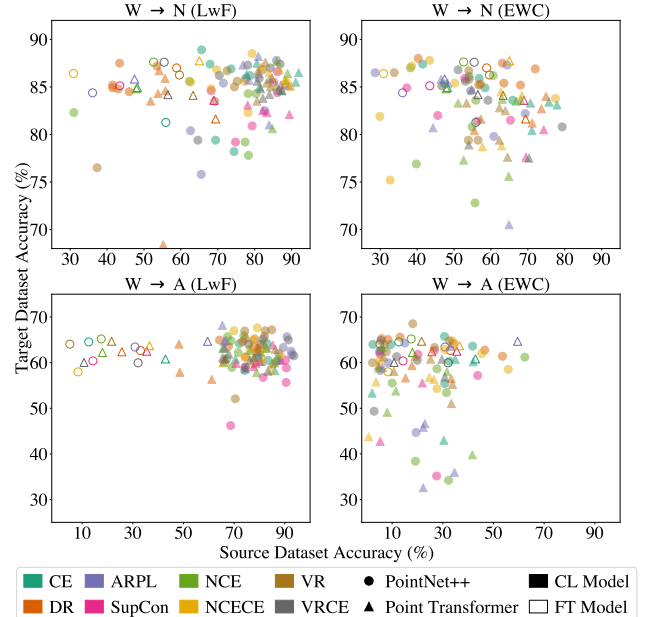


Figure 2. Continual learning performance on Waymo-to-NuScenes and Waymo-to-Argoverse2 under different λ values.

trophic forgetting. In contrast, LwF generally preserved higher source accuracy than FT (except for DR models in W→N), showing that maintaining base model predictions on target samples—even without source memory—can effectively reduce forgetting.

The advantage of SSL objectives in LP did not translate to CL. **SSL models are not superior to supervised ones**

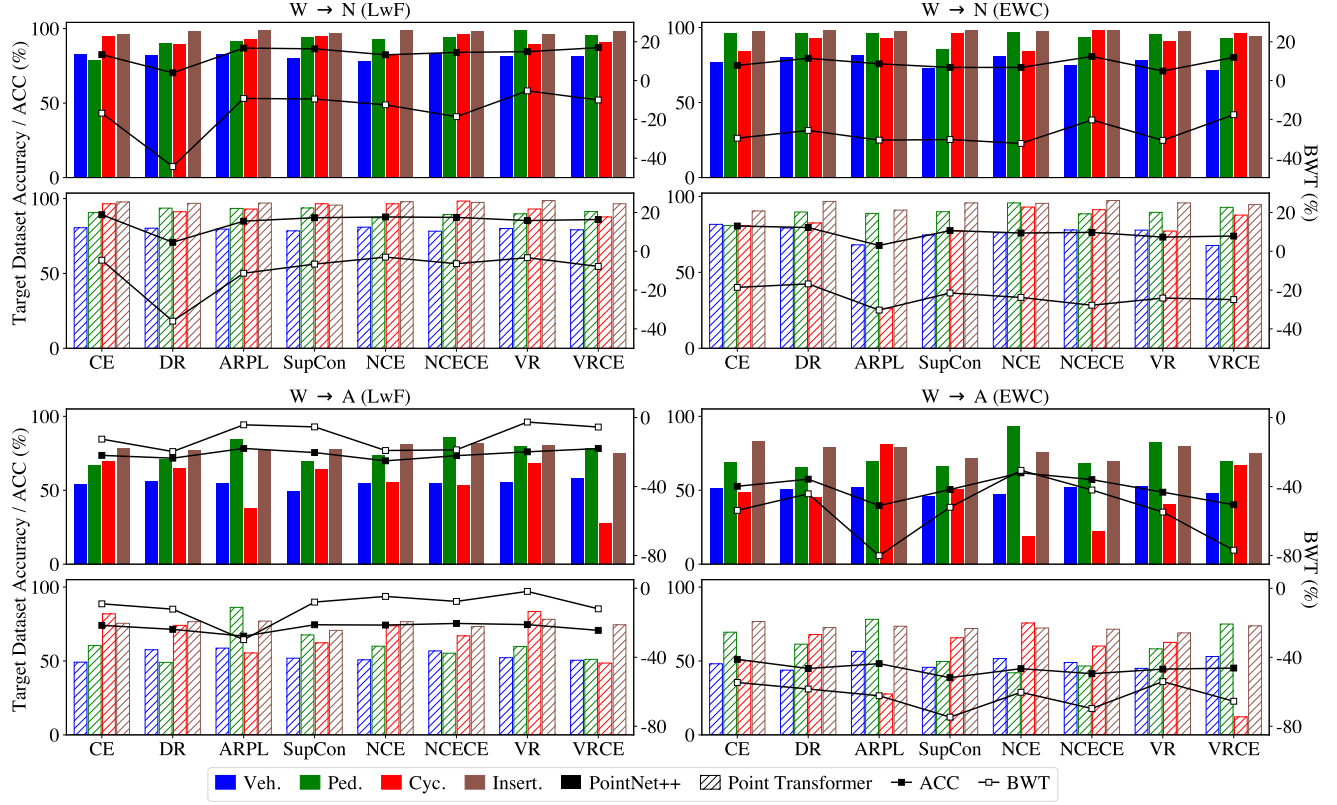


Figure 3. Continual Learning performance on Waymo-to-NuScenes (Row 1) and Waymo-to-Argoverse2 (Row 2). Column 1 shows LwF models, and Column 2 shows EWC models. Veh., Ped., and Cyc. denote the vehicle, pedestrian, and cyclist classes, respectively.

in CL; for example, in $W \rightarrow N$ with Point Transformer, CE achieved higher ACC than SSL models. While base models exhibited feature spaces that varied substantially by objective (Fig. 8), these differences became less pronounced in CL models (Fig. 7).

DR models perform notably worse under LwF, due to their strong tendency toward neural collapse [40], which preserves only class prototypes while discarding intra-class variation. This made them highly susceptible to forgetting when old and new tasks overlap in feature space [16, 51], especially in class-split cases (e.g., Waymo vehicle vs. NuScenes sub-vehicles). To quantify this, we measured Maximum Mean Discrepancy (MMD) and cosine simi-

larity between Waymo and NuScenes vehicle samples in the penultimate feature space of the PointNet++ models (Tab. 6). DR models showed the strongest overlap, with lower MMD and higher cosine similarity than other models. Interestingly, this weakness was absent under EWC: while LwF primarily enforces logit alignment, EWC constrains parameters across layers, enabling knowledge retention beyond collapsed prototypes.

3.3. Domain Gap Reduction via Pre-Processing

We employed line downsampling [66] and bounding box normalization to address domain gaps not handled in Open-

| | MMD $\times 10^{-4}$ | Cos-Sim. | MMD $\times 10^{-4}$ | Cos-Sim. |
|--------|-------------------------|----------|-------------------------|----------|
| CE | 10.1 | 0.97 | NCE | 13.1 |
| DR | 2.8 | 0.99 | NCECE | 7.1 |
| ARPL | 15.6 | 0.97 | VR | 20.7 |
| SupCon | 1.0 | 0.97 | VRCE | 154.3 |

Table 6. Overlap between Waymo and NuScenes dataset in vehicle samples in terms of **MMD** and cosine similarity (**Cos-Sim.**).

| | Waymo | NuScenes | Argoverse2 |
|-----------------------------------------------------|-------------|-------------|-------------|
| + Line Downsampling | 95.6 | 89.8 | 75.7 |
| + Bounding Box Normalization | 96.7 | 85.9 | 74.3 |
| + Line Downsampling - Bounding Box Normalization | 96.1 | 89.2 | 79.0 |

Table 7. Accuracies(%) of ablation study on data preprocessing: Line downsampling and bounding box normalization.

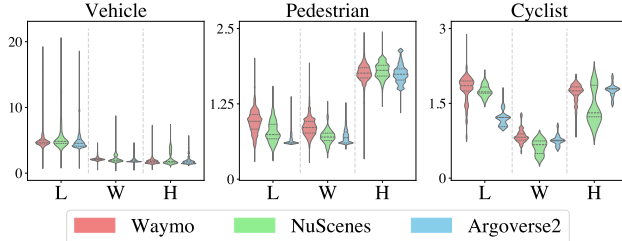


Figure 4. Distribution of 3D bounding box dimensions (length, width, height) in Waymo, NuScenes, and Argoverse2 datasets.

PCDet [58]. Line downsampling improved zero-shot transfer to NuScenes and Argoverse2 despite lowering Waymo validation accuracy (Tab. 7). Bounding box normalization, however, had different effects. While differences in (l, w, h) provides useful cues for object classification in each dataset, it can bias the model toward the training dataset. Its impact varied across transfer: it improved $W \rightarrow N$ but slightly degraded $W \rightarrow A$, largely due to cyclists—NuScenes included a bimodal height distribution where the lower mode corresponds to riderless bicycles (Fig. 4). Normalization thus benefited $W \rightarrow N$ by handling this class expansion.

3.4. Stability Issues in EWC

EWC showed high sensitivity to λ , with large variance in source and target accuracies (Fig. 2). Similar observations were reported in [28], where neurons in convolutional and attention layers—core components of PointNet++ and Point Transformer, respectively—have larger importance scores than linear layers, negatively affecting convergence. Stabilization strategies may be needed for such backbones, which we leave for future work.

We also found that the Point Transformer ARPL model under EWC has low target accuracies, especially for the cyclist class. As shown in Fig. 5, its importance scores were concentrated in a few intermediate neurons rather than the bimodal distribution seen in other models, causing excessive regularization and a training bottleneck. This highlights a limitation of standard EWC FIM calculation, suggesting that layer-aware regularization [54] could improve stability.

4. Related Work

Continual Learning Continual learning (CL) enables models to learn sequential tasks without forgetting prior knowledge, with techniques to prevent catastrophic forgetting [37]. Regularization-based methods constrain parameter updates to preserve past knowledge, e.g., EWC [26] uses the Fisher Information Matrix to estimate the importance of each neuron to regularize, while LwF [32] applies knowledge distillation at the last layer outputs. Recent CL studies in 3D point clouds [7, 18, 48, 57] largely follow 2D image-

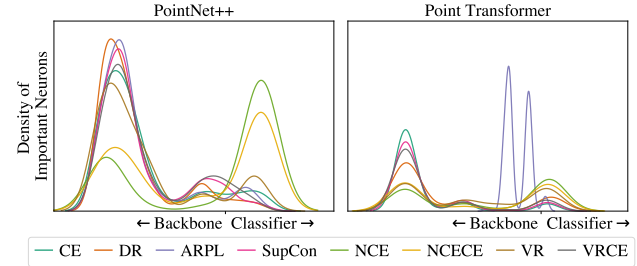


Figure 5. Distribution of important neuron across layers in terms of the importance score in EWC. 1000 most important neurons are selected for each model to draw KDE plots.

domain setups. Although [57] considers both domain shift and CIL, it assumes dense points (≥ 1024 points) and disjoint classes across tasks, limiting real-world applicability. Our work investigates CL under joint domain and diverse label shifts in LiDAR datasets.

3D Point Cloud Recognition Deep learning methods for 3D point clouds are commonly grouped into projection-, voxel-, and point-based approaches. Projection-based methods map points to 2D views for CNNs [14, 29, 55], often losing geometric detail. Voxel-based methods discretize space for 3D convolutions [36, 53], with sparse variants improving efficiency [15, 20], though scalability remains limited. Point-based methods directly process raw points [34, 43, 44, 59, 74], and recent works integrate transformers for long-range dependencies [22, 68, 69, 75]. We adopt PointNet++ [44] and Point Transformer [75] as baselines, representing convolution- and attention-based architectures.

Generalizability in Representation Learning Generalizable representations are essential for transfer across domains and tasks. While supervised learning achieves strong task-specific performance, it often fails under domain shifts or novel labels. Self-supervised learning (SSL) leverages unlabeled data [4, 9, 13, 60] and typically yields more transferable features, sometimes surpassing supervised models [76]. Yet, generalizability is usually evaluated in static settings (e.g., zero-shot, linear probe) [45], leaving its reliability under continual learning (CL) with domain and label shifts less explored. Our results show that SSL models often underperform in CL, highlighting the need to reassess representation robustness in dynamic scenarios.

5. Conclusion & Future Directions

We introduced ROAD, a benchmark for 3D perception that jointly addresses domain and label shifts. Through evaluations of multiple knowledge transfer tasks across two realistic scenarios—Waymo-to-NuScenes and Waymo-to-Argoverse2—we showed that backbone choice, training objectives, and CL strategies significantly affect adaptability. Our benchmark offers insights for building ro-

bust 3D perception systems and may also inform research in other 3D domains, given the sparsity and difficulty of LiDAR point clouds. Future work includes extending our study with stronger backbones, advanced pre-training and CL approaches, and scaling to more challenging tasks such as 3D object detection and motion forecasting.

References

[1] Rahaf Aljundi, Klaas Kelchtermans, and Tinne Tuytelaars. Task-free continual learning. In *IEEE Conference on Computer Vision and Pattern Recognition, CVPR 2019, Long Beach, CA, USA, June 16-20, 2019*, pages 11254–11263. Computer Vision Foundation / IEEE, 2019. 1

[2] Bang An, Zora Che, Mucong Ding, and Furong Huang. Transferring fairness under distribution shifts via fair consistency regularization. In *Advances in Neural Information Processing Systems 35: Annual Conference on Neural Information Processing Systems 2022, NeurIPS 2022, New Orleans, LA, USA, November 28 - December 9, 2022*, 2022. 2

[3] Jihwan Bang, Heesu Kim, Youngjoon Yoo, Jung-Woo Ha, and Jonghyun Choi. Rainbow memory: Continual learning with a memory of diverse samples. In *IEEE Conference on Computer Vision and Pattern Recognition, CVPR 2021, virtual, June 19-25, 2021*, pages 8218–8227. Computer Vision Foundation / IEEE, 2021. 1

[4] Adrien Bardes, Jean Ponce, and Yann LeCun. Vi-creg: Variance-invariance-covariance regularization for self-supervised learning. In *The Tenth International Conference on Learning Representations, ICLR 2022, Virtual Event, April 25-29, 2022*. OpenReview.net, 2022. 4, 8, 13

[5] Pietro Buzzega, Matteo Boschini, Angelo Porrello, Davide Abati, and Simone Calderara. Dark experience for general continual learning: a strong, simple baseline. In *Advances in Neural Information Processing Systems 33: Annual Conference on Neural Information Processing Systems 2020, NeurIPS 2020, December 6-12, 2020, virtual*, 2020. 1

[6] Holger Caesar, Varun Bankiti, Alex H. Lang, Sourabh Vora, Venice Erin Liang, Qiang Xu, Anush Krishnan, Yu Pan, Giacarlo Baldan, and Oscar Beijbom. nuscenes: A multimodal dataset for autonomous driving. In *2020 IEEE/CVF Conference on Computer Vision and Pattern Recognition, CVPR 2020, Seattle, WA, USA, June 13-19, 2020*, pages 11618–11628. Computer Vision Foundation / IEEE, 2020. 1, 2, 3, 4

[7] Elena Camuffo and Simone Milani. Continual learning for lidar semantic segmentation: Class-incremental and coarse-to-fine strategies on sparse data. *CoRR*, abs/2304.03980, 2023. 8

[8] Haozhi Cao, Yuecong Xu, Jianfei Yang, Pengyu Yin, Shenghai Yuan, and Lihua Xie. Multi-modal continual test-time adaptation for 3d semantic segmentation. In *IEEE/CVF International Conference on Computer Vision, ICCV 2023, Paris, France, October 1-6, 2023*, pages 18763–18773. IEEE, 2023. 1

[9] Mathilde Caron, Ishan Misra, Julien Mairal, Priya Goyal, Piotr Bojanowski, and Armand Joulin. Unsupervised learning of visual features by contrasting cluster assignments. In *Advances in Neural Information Processing Systems 33: Annual Conference on Neural Information Processing Systems 2020, NeurIPS 2020, December 6-12, 2020, virtual*, 2020. 8

[10] Antonio Carta, Lorenzo Pellegrini, Andrea Cossu, Hamed Hemati, and Vincenzo Lomonaco. Avalanche: A pytorch library for deep continual learning. *J. Mach. Learn. Res.*, 24:363:1–363:6, 2023. 5

[11] Francisco M. Castro, Manuel J. Marín-Jiménez, Nicolás Guil, Cordelia Schmid, and Karteek Alahari. End-to-end incremental learning. In *Computer Vision - ECCV 2018 - 15th European Conference, Munich, Germany, September 8-14, 2018, Proceedings, Part XII*, pages 241–257. Springer, 2018. 1

[12] Guangyao Chen, Peixi Peng, Xiangqian Wang, and Yonghong Tian. Adversarial reciprocal points learning for open set recognition. *IEEE Trans. Pattern Anal. Mach. Intell.*, 44(11):8065–8081, 2022. 4, 13

[13] Ting Chen, Simon Kornblith, Mohammad Norouzi, and Geoffrey E. Hinton. A simple framework for contrastive learning of visual representations. In *Proceedings of the 37th International Conference on Machine Learning, ICML 2020, 13-18 July 2020, Virtual Event*, pages 1597–1607. PMLR, 2020. 4, 8

[14] Xiaozhi Chen, Huimin Ma, Ji Wan, Bo Li, and Tian Xia. Multi-view 3d object detection network for autonomous driving. In *2017 IEEE Conference on Computer Vision and Pattern Recognition, CVPR 2017, Honolulu, HI, USA, July 21-26, 2017*, pages 6526–6534. IEEE Computer Society, 2017. 8

[15] Christopher B. Choy, JunYoung Gwak, and Silvio Savarese. 4d spatio-temporal convnets: Minkowski convolutional neural networks. In *IEEE Conference on Computer Vision and Pattern Recognition, CVPR 2019, Long Beach, CA, USA, June 16-20, 2019*, pages 3075–3084. Computer Vision Foundation / IEEE, 2019. 8

[16] Trung-Anh Dang, Vincent Nguyen, Ngoc-Son Vu, and Christel Vrain. Memory-efficient continual learning with neural collapse contrastive. In *IEEE/CVF Winter Conference on Applications of Computer Vision, WACV 2025, Tucson, AZ, USA, February 26 - March 6, 2025*, pages 7950–7959. IEEE, 2025. 7

[17] Jiahua Dong, Yang Cong, Gan Sun, Lixu Wang, Lingjuan Lyu, Jun Li, and Ender Konukoglu. Inor-net: Incremental 3-d object recognition network for point cloud representation. *IEEE Trans. Neural Networks Learn. Syst.*, 34(10):6955–6967, 2023. 4

[18] George Eskandar. An empirical study of the generalization ability of lidar 3d object detectors to unseen domains. In *IEEE/CVF Conference on Computer Vision and Pattern Recognition, CVPR 2024, Seattle, WA, USA, June 16-22, 2024*, pages 23815–23825. IEEE, 2024. 1, 2, 4, 8

[19] Alexander Gepperth and Barbara Hammer. Incremental learning algorithms and applications. In *24th European Symposium on Artificial Neural Networks, ESANN 2016, Bruges, Belgium, April 27-29, 2016*, 2016. 1

[20] Benjamin Graham, Martin Engelcke, and Laurens van der Maaten. 3d semantic segmentation with submanifold sparse

convolutional networks. In *2018 IEEE Conference on Computer Vision and Pattern Recognition, CVPR 2018, Salt Lake City, UT, USA, June 18-22, 2018*, pages 9224–9232. Computer Vision Foundation / IEEE Computer Society, 2018. 8

[21] Li Guo, George Andriopoulos, Zifan Zhao, Zixuan Dong, Shuyang Ling, and Keith W. Ross. Cross entropy versus label smoothing: A neural collapse perspective. *Trans. Mach. Learn. Res.*, 2025, 2025. 1, 4

[22] Meng-Hao Guo, Junxiong Cai, Zheng-Ning Liu, Tai-Jiang Mu, Ralph R. Martin, and Shi-Min Hu. PCT: point cloud transformer. *Comput. Vis. Media*, 7(2):187–199, 2021. 8

[23] Nong Minh Hieu, Antoine Ledent, Yunwen Lei, and Cheng Yeaw Ku. Generalization analysis for deep contrastive representation learning. In *AAAI-25, Sponsored by the Association for the Advancement of Artificial Intelligence, February 25 - March 4, 2025, Philadelphia, PA, USA*, pages 17186–17194. AAAI Press, 2025. 4

[24] Carlos Nascimento Silla Jr. and Alex Alves Freitas. A survey of hierarchical classification across different application domains. *Data Min. Knowl. Discov.*, 22(1-2):31–72, 2011. 2

[25] Prannay Khosla, Piotr Teterwak, Chen Wang, Aaron Sarna, Yonglong Tian, Phillip Isola, Aaron Maschinot, Ce Liu, and Dilip Krishnan. Supervised contrastive learning. In *Advances in Neural Information Processing Systems 33: Annual Conference on Neural Information Processing Systems 2020, NeurIPS 2020, December 6-12, 2020, virtual*, 2020. 4

[26] James Kirkpatrick, Razvan Pascanu, Neil C. Rabinowitz, Joel Veness, Guillaume Desjardins, Andrei A. Rusu, Kieran Milan, John Quan, Tiago Ramalho, Agnieszka Grabska-Barwinska, Demis Hassabis, Claudia Clopath, Dharshan Kumaran, and Raia Hadsell. Overcoming catastrophic forgetting in neural networks. *CoRR*, abs/1612.00796, 2016. 4, 8

[27] Hyunseo Koh, Dahyun Kim, Jung-Woo Ha, and Jonghyun Choi. Online continual learning on class incremental blurry task configuration with anytime inference. In *The Tenth International Conference on Learning Representations, ICLR 2022, Virtual Event, April 25-29, 2022*. OpenReview.net, 2022. 1

[28] Alexey Kutalev and Alisa Lapina. Stabilizing elastic weight consolidation method in practical ML tasks and using weight importances for neural network pruning. *CoRR*, abs/2109.10021, 2021. 8

[29] Alex H. Lang, Sourabh Vora, Holger Caesar, Lubing Zhou, Jiong Yang, and Oscar Beijbom. Pointpillars: Fast encoders for object detection from point clouds. In *IEEE Conference on Computer Vision and Pattern Recognition, CVPR 2019, Long Beach, CA, USA, June 16-20, 2019*, pages 12697–12705. Computer Vision Foundation / IEEE, 2019. 8

[30] Byung Hyun Lee, Okchul Jung, Jonghyun Choi, and Se Young Chun. Online continual learning on hierarchical label expansion. In *IEEE/CVF International Conference on Computer Vision, ICCV 2023, Paris, France, October 1-6, 2023*, pages 11727–11736. IEEE, 2023. 1

[31] Timothée Lesort. *Apprentissage continu : S'attaquer à l'oubli foudroyant des réseaux de neurones profonds grâce aux méthodes à rejeter de données. (Continual Learning : Tackling Catastrophic Forgetting in Deep Neural Networks with Replay Processes)*. PhD thesis, Institut Polytechnique de Paris, France, 2020. 14

[32] Zhizhong Li and Derek Hoiem. Learning without forgetting. In *Computer Vision - ECCV 2016 - 14th European Conference, Amsterdam, The Netherlands, October 11-14, 2016, Proceedings, Part IV*, pages 614–629. Springer, 2016. 4, 8

[33] David Lopez-Paz and Marc’Aurelio Ranzato. Gradient episodic memory for continual learning. In *Advances in Neural Information Processing Systems 30: Annual Conference on Neural Information Processing Systems 2017, December 4-9, 2017, Long Beach, CA, USA*, pages 6467–6476, 2017. 4, 14

[34] Xu Ma, Can Qin, Haoxuan You, Haoxi Ran, and Yun Fu. Rethinking network design and local geometry in point cloud: A simple residual MLP framework. In *The Tenth International Conference on Learning Representations, ICLR 2022, Virtual Event, April 25-29, 2022*. OpenReview.net, 2022. 8

[35] Yeganeh Madadi, Vahid Seydi, Kamal Nasrollahi, Reshad Hosseini, and Thomas B. Moeslund. Deep visual unsupervised domain adaptation for classification tasks: a survey. *IET Image Process.*, 14(14):3283–3299, 2020. 2

[36] Daniel Maturana and Sebastian A. Scherer. Voxnet: A 3d convolutional neural network for real-time object recognition. In *2015 IEEE/RSJ International Conference on Intelligent Robots and Systems, IROS 2015, Hamburg, Germany, September 28 - October 2, 2015*, pages 922–928. IEEE, 2015. 8

[37] Michael McCloskey and Neal J Cohen. Catastrophic interference in connectionist networks: The sequential learning problem. In *Psychology of learning and motivation*, pages 109–165. Elsevier, 1989. 8

[38] Björn Michele, Alexandre Boulch, Tuan-Hung Vu, Gilles Puy, Renaud Marlet, and Nicolas Courty. Train till you drop: Towards stable and robust source-free unsupervised 3d domain adaptation. In *Computer Vision - ECCV 2024 - 18th European Conference, Milan, Italy, September 29-October 4, 2024, Proceedings, Part XX*, pages 1–19. Springer, 2024. 3

[39] Shishir Muralidhara, Saqib Bukhari, Georg Schneider, Dieder Stricker, and René Schuster. CLEO: continual learning of evolving ontologies. In *Computer Vision - ECCV 2024 - 18th European Conference, Milan, Italy, September 29-October 4, 2024, Proceedings, Part LIV*, pages 328–344. Springer, 2024. 3

[40] Vardan Papyan, X. Y. Han, and David L. Donoho. Prevalence of neural collapse during the terminal phase of deep learning training. *CoRR*, abs/2008.08186, 2020. 7

[41] Adam Paszke, Sam Gross, Francisco Massa, Adam Lerer, James Bradbury, Gregory Chanan, Trevor Killeen, Zeming Lin, Natalia Gimelshein, Luca Antiga, Alban Desmaison, Andreas Köpf, Edward Z. Yang, Zachary DeVito, Martin Raison, Alykhan Tejani, Sasank Chilamkurthy, Benoit Steiner, Lu Fang, Junjie Bai, and Soumith Chintala. Pytorch: An imperative style, high-performance deep learning library. In *Advances in Neural Information Processing Systems 32: Annual Conference on Neural Information Processing Systems*

tems 2019, NeurIPS 2019, December 8-14, 2019, Vancouver, BC, Canada, pages 8024–8035, 2019. 13

[42] F. Pedregosa, G. Varoquaux, A. Gramfort, V. Michel, B. Thirion, O. Grisel, M. Blondel, P. Prettenhofer, R. Weiss, V. Dubourg, J. Vanderplas, A. Passos, D. Cournapeau, M. Brucher, M. Perrot, and E. Duchesnay. Scikit-learn: Machine learning in Python. *Journal of Machine Learning Research*, 12:2825–2830, 2011. 14

[43] Charles Ruizhongtai Qi, Hao Su, Kaichun Mo, and Leonidas J. Guibas. Pointnet: Deep learning on point sets for 3d classification and segmentation. In *2017 IEEE Conference on Computer Vision and Pattern Recognition, CVPR 2017, Honolulu, HI, USA, July 21-26, 2017*, pages 77–85. IEEE Computer Society, 2017. 8

[44] Charles Ruizhongtai Qi, Li Yi, Hao Su, and Leonidas J. Guibas. Pointnet++: Deep hierarchical feature learning on point sets in a metric space. In *Advances in Neural Information Processing Systems 30: Annual Conference on Neural Information Processing Systems 2017, December 4-9, 2017, Long Beach, CA, USA*, pages 5099–5108, 2017. 4, 8, 13

[45] Alec Radford, Jong Wook Kim, Chris Hallacy, Aditya Ramesh, Gabriel Goh, Sandhini Agarwal, Girish Sastry, Amanda Askell, Pamela Mishkin, Jack Clark, Gretchen Krueger, and Ilya Sutskever. Learning transferable visual models from natural language supervision. In *Proceedings of the 38th International Conference on Machine Learning, ICML 2021, 18-24 July 2021, Virtual Event*, pages 8748–8763. PMLR, 2021. 8

[46] Sylvestre-Alvise Rebiffé, Alexander Kolesnikov, Georg Sperl, and Christoph H. Lampert. icarl: Incremental classifier and representation learning. In *2017 IEEE Conference on Computer Vision and Pattern Recognition, CVPR 2017, Honolulu, HI, USA, July 21-26, 2017*, pages 5533–5542. IEEE Computer Society, 2017. 1

[47] Hossein Resani and Behrooz Nasihatkon. MIRACLE 3d: Memory-efficient integrated robust approach for continual learning on 3d point clouds via shape model construction. In *The Thirteenth International Conference on Learning Representations, ICLR 2025, Singapore, April 24-28, 2025*. OpenReview.net, 2025. 4

[48] Hossein Resani, Behrooz Nasihatkon, and Mohammadmreza Alimoradi Jazi. Continual learning in 3d point clouds: Employing spectral techniques for exemplar selection. In *IEEE/CVF Winter Conference on Applications of Computer Vision, WACV 2025, Tucson, AZ, USA, February 26 - March 6, 2025*, pages 2921–2931. IEEE, 2025. 4, 8

[49] David Rolnick, Arun Ahuja, Jonathan Schwarz, Timothy P. Lillicrap, and Gregory Wayne. Experience replay for continual learning. In *Advances in Neural Information Processing Systems 32: Annual Conference on Neural Information Processing Systems 2019, NeurIPS 2019, December 8-14, 2019, Vancouver, BC, Canada*, pages 348–358, 2019. 2, 14

[50] Nikunj Saunshi, Orestis Plevrakis, Sanjeev Arora, Mikhail Khodak, and Hrishikesh Khandeparkar. A theoretical analysis of contrastive unsupervised representation learning. In *Proceedings of the 36th International Conference on Machine Learning, ICML 2019, 9-15 June 2019, Long Beach, California, USA*, pages 5628–5637. PMLR, 2019. 4

[51] Minhyuk Seo, Hyunseo Koh, Wonje Jeung, Minjae Lee, San Kim, Hankook Lee, Sungjun Cho, Sungik Choi, Hyunwoo Kim, and Jonghyun Choi. Learning equi-angular representations for online continual learning. In *IEEE/CVF Conference on Computer Vision and Pattern Recognition, CVPR 2024, Seattle, WA, USA, June 16-22, 2024*, pages 23933–23942. IEEE, 2024. 7

[52] Christian Simon, Masoud Faraki, Yi-Hsuan Tsai, Xiang Yu, Samuel Schulter, Yumin Suh, Mehrtash Harandi, and Manmohan Chandraker. On generalizing beyond domains in cross-domain continual learning. In *IEEE/CVF Conference on Computer Vision and Pattern Recognition, CVPR 2022, New Orleans, LA, USA, June 18-24, 2022*, pages 9255–9264. IEEE, 2022. 1

[53] Shuran Song, Fisher Yu, Andy Zeng, Angel X. Chang, Manolis Savva, and Thomas A. Funkhouser. Semantic scene completion from a single depth image. In *2017 IEEE Conference on Computer Vision and Pattern Recognition, CVPR 2017, Honolulu, HI, USA, July 21-26, 2017*, pages 190–198. IEEE Computer Society, 2017. 8

[54] Shezheng Song, Hao Xu, Jun Ma, Shasha Li, Long Peng, Qian Wang, Xiaodong Liu, and Jie Yu. How to complete domain tuning while keeping general ability in LLM: adaptive layer-wise and element-wise regularization. *CoRR*, abs/2501.13669, 2025. 8

[55] Hang Su, Subhransu Maji, Evangelos Kalogerakis, and Erik G. Learned-Miller. Multi-view convolutional neural networks for 3d shape recognition. In *2015 IEEE International Conference on Computer Vision, ICCV 2015, Santiago, Chile, December 7-13, 2015*, pages 945–953. IEEE Computer Society, 2015. 8

[56] Pei Sun, Henrik Kretzschmar, Xerxes Dotiwalla, Aurelien Chouard, Vijaysai Patnaik, Paul Tsui, James Guo, Yin Zhou, Yuning Chai, Benjamin Caine, Vijay Vasudevan, Wei Han, Jiquan Ngiam, Hang Zhao, Aleksei Timofeev, Scott Ettinger, Maxim Krivokon, Amy Gao, Aditya Joshi, Yu Zhang, Jonathon Shlens, Zhifeng Chen, and Dragomir Anguelov. Scalability in perception for autonomous driving: Waymo open dataset. In *2020 IEEE/CVF Conference on Computer Vision and Pattern Recognition, CVPR 2020, Seattle, WA, USA, June 13-19, 2020*, pages 2443–2451. Computer Vision Foundation / IEEE, 2020. 1, 2, 3, 4

[57] Yuwen Tan and Xiang Xiang. Cross-domain few-shot incremental learning for point-cloud recognition. In *IEEE/CVF Winter Conference on Applications of Computer Vision, WACV 2024, Waikoloa, HI, USA, January 3-8, 2024*, pages 2296–2305. IEEE, 2024. 4, 8

[58] OpenPCDet Development Team. Openpcdet: An open-source toolbox for 3d object detection from point clouds. <https://github.com/open-mmlab/OpenPCDet>, 2020. 4, 8

[59] Hugues Thomas, Charles R. Qi, Jean-Emmanuel Deschaud, Beatriz Marcotegui, François Goulette, and Leonidas J. Guibas. Kpconv: Flexible and deformable convolution for point clouds. In *2019 IEEE/CVF International Conference on Computer Vision, ICCV 2019, Seoul, Korea (South), October 27 - November 2, 2019*, pages 6410–6419. IEEE, 2019. 8

[60] Aäron van den Oord, Yazhe Li, and Oriol Vinyals. Representation learning with contrastive predictive coding. *CoRR*, abs/1807.03748, 2018. 8

[61] Liyuan Wang, Xingxing Zhang, Hang Su, and Jun Zhu. A comprehensive survey of continual learning: Theory, method and application. *IEEE Trans. Pattern Anal. Mach. Intell.*, 46(8):5362–5383, 2024. 1

[62] Mei Wang and Weihong Deng. Deep visual domain adaptation: A survey. *Neurocomputing*, 312:135–153, 2018. 1

[63] Wei Wang, Vincent W. Zheng, Han Yu, and Chunyan Miao. A survey of zero-shot learning: Settings, methods, and applications. *ACM Trans. Intell. Syst. Technol.*, 10(2):13:1–13:37, 2019. 1

[64] Yaqing Wang, Quanming Yao, James T. Kwok, and Lionel M. Ni. Generalizing from a few examples: A survey on few-shot learning. *ACM Comput. Surv.*, 53(3):63:1–63:34, 2021. 1

[65] Yan Wang, Junbo Yin, Wei Li, Pascal Frossard, Ruigang Yang, and Jianbing Shen. SSDA3D: semi-supervised domain adaptation for 3d object detection from point cloud. In *Thirty-Seventh AAAI Conference on Artificial Intelligence, AAAI 2023, Thirty-Fifth Conference on Innovative Applications of Artificial Intelligence, IAAI 2023, Thirteenth Symposium on Educational Advances in Artificial Intelligence, EAAI 2023, Washington, DC, USA, February 7-14, 2023*, pages 2707–2715. AAAI Press, 2023. 1

[66] Yi Wei, Zibu Wei, Yongming Rao, Jiaxin Li, Jie Zhou, and Jiwen Lu. Lidar distillation: Bridging the beam-induced domain gap for 3d object detection. In *Computer Vision - ECCV 2022 - 17th European Conference, Tel Aviv, Israel, October 23-27, 2022, Proceedings, Part XXXIX*, pages 179–195. Springer, 2022. 2, 5, 7

[67] Benjamin Wilson, William Qi, Tanmay Agarwal, John Lambert, Jagjeet Singh, Siddhesh Khandelwal, Bowen Pan, Ratnesh Kumar, Andrew Hartnett, Jhony Kaesemeyer Pontes, Deva Ramanan, Peter Carr, and James Hays. Argoverse 2: Next generation datasets for self-driving perception and forecasting. In *Proceedings of the Neural Information Processing Systems Track on Datasets and Benchmarks 1, NeurIPS Datasets and Benchmarks 2021, December 2021, virtual*, 2021. 2, 3, 4

[68] Xiaoyang Wu, Yixing Lao, Li Jiang, Xihui Liu, and Hengshuang Zhao. Point transformer V2: grouped vector attention and partition-based pooling. In *Advances in Neural Information Processing Systems 35: Annual Conference on Neural Information Processing Systems 2022, NeurIPS 2022, New Orleans, LA, USA, November 28 - December 9, 2022*, 2022. 8

[69] Xiaoyang Wu, Li Jiang, Peng-Shuai Wang, Zhijian Liu, Xihui Liu, Yu Qiao, Wanli Ouyang, Tong He, and Hengshuang Zhao. Point transformer V3: simpler, faster, stronger. In *IEEE/CVF Conference on Computer Vision and Pattern Recognition, CVPR 2024, Seattle, WA, USA, June 16-22, 2024*, pages 4840–4851. IEEE, 2024. 8

[70] Jiangwei Xie, Shipeng Yan, and Xuming He. General incremental learning with domain-aware categorical representations. In *IEEE/CVF Conference on Computer Vision and Pattern Recognition, CVPR 2022, New Orleans, LA, USA, June 18-24, 2022*, pages 14331–14340. IEEE, 2022. 1

[71] Yibo Yang, Shixiang Chen, Xiangtai Li, Liang Xie, Zhouchen Lin, and Dacheng Tao. Inducing neural collapse in imbalanced learning: Do we really need a learnable classifier at the end of deep neural network? In *Advances in Neural Information Processing Systems 35: Annual Conference on Neural Information Processing Systems 2022, NeurIPS 2022, New Orleans, LA, USA, November 28 - December 9, 2022*, 2022. 4

[72] Maciej Zamorski, Michał Stypulkowski, Konrad Karanowski, Tomasz Trzcinski, and Maciej Zieba. Continual learning on 3d point clouds with random compressed rehearsal. *Comput. Vis. Image Underst.*, 228:103621, 2023. 4

[73] Bo Zhang, Xinyu Cai, Jiakang Yuan, Donglin Yang, Jianfei Guo, Xiangchao Yan, Renqiu Xia, Botian Shi, Min Dou, Tao Chen, Si Liu, Junchi Yan, and Yu Qiao. Resimad: Zero-shot 3d domain transfer for autonomous driving with source reconstruction and target simulation. In *The Twelfth International Conference on Learning Representations, ICLR 2024, Vienna, Austria, May 7-11, 2024*. OpenReview.net, 2024. 1, 2

[74] Hengshuang Zhao, Li Jiang, Chi-Wing Fu, and Jiaya Jia. Pointweb: Enhancing local neighborhood features for point cloud processing. In *IEEE Conference on Computer Vision and Pattern Recognition, CVPR 2019, Long Beach, CA, USA, June 16-20, 2019*, pages 5565–5573. Computer Vision Foundation / IEEE, 2019. 8

[75] Hengshuang Zhao, Li Jiang, Jiaya Jia, Philip H. S. Torr, and Vladlen Koltun. Point transformer. In *2021 IEEE/CVF International Conference on Computer Vision, ICCV 2021, Montreal, QC, Canada, October 10-17, 2021*, pages 16239–16248. IEEE, 2021. 4, 8, 13

[76] Nanxuan Zhao, Zhirong Wu, Rynson W. H. Lau, and Stephen Lin. What makes instance discrimination good for transfer learning? In *9th International Conference on Learning Representations, ICLR 2021, Virtual Event, Austria, May 3-7, 2021*. OpenReview.net, 2021. 8

[77] Da-Wei Zhou, Fu-Yun Wang, Han-Jia Ye, and De-Chuan Zhan. Pycil: a python toolbox for class-incremental learning. *Sci. China Inf. Sci.*, 66(9), 2023. 5

A. Implementation Details

All experiments were conducted using an NVIDIA A100 GPU and PyTorch [41] version 1.12.1 with CUDA 11.3. For optimization, we used the Adam optimizer with a weight decay of 0.01 and a momentum of 0.9, while other hyperparameters were set to their default values in the PyTorch package. Training epochs were chosen to ensure sufficient convergence of the loss. With a batch size of 128, base models converged after approximately 80K iterations. LP fine-tuning required 9K and 15K iterations for NuScenes and Argoverse2, respectively, while CL training required 19K and 30K iterations. The latest checkpoints were used for evaluation.

A.1. Dataset Description

Tab. 9 provides class-wise number of samples of the training and validation datasets, after the pre-processing mentioned in the experimental section. For source and target class selection, we followed the default setting of OpenPCDet. We further excluded four classes (`construction_cone`, `dog`, `message_board_trailer`, and `wheelchair`) for Argoverse2, whose frequency is below 0.02% in the training set after discarding the objects with number of points under 64.

A.2. Model Architectures

The model architecture consists of a PointNet++ [44] or Point Transformer [75] backbone followed by a 4-layer fully connected classifier head with output dimensions of $[512, 256, 128, num_classes]$, where each layer includes Batch Normalization and ReLU activation.

PointNet++ employs a stacked multi-scale grouping (MSG) configuration defined as follows (notation follows the original PointNet++ paper): $SA(K, r, [l_1, \dots, l_d])$ denotes a Set Abstraction (SA) level with K local regions of ball radius r , using PointNet with d fully connected layers of widths l_i . $SA([l_1, \dots, l_d])$ represents a global SA level aggregating the entire set into a single vector. For multi-scale settings, $SA(K, [r^{(1)}, \dots, r^{(m)}], [[l_1^{(1)}, \dots, l_d^{(1)}], \dots, [l_1^{(m)}, \dots, l_d^{(m)}]])$ indicates MSG with m radii and corresponding MLPs. Our specific architecture for PointNet++ backbone is:

| Layer | Configuration |
|-------|-----------------------------------------------------------------------------|
| SA 1 | 256, $[0.1, 0.2, 0.4]$, $[[32, 32, 64], [64, 64, 128], [64, 96, 128]]$ |
| SA 2 | 64, $[0.2, 0.4, 0.8]$, $[[64, 64, 128], [128, 128, 256], [128, 128, 256]]$ |
| SA 3 | 16, 1.0, $[256, 512, 1024]$ |

Table 8. PointNet++ model architecture.

Point Transformer employs residual transformer blocks composed of self-attention and linear projection layers, followed by downsampling. We stacked five encoder blocks

with downsampling rates $[1, 2, 2, 4, 4]$, producing point set sizes $[N, N/2, N/4, N/16, N/64]$, where N is the number of input points. All other hyperparameters followed the original implementation [75].

A.3. Base Objectives

For self-supervised learning (SSL) objectives, the penultimate feature layer—i.e., the output after the third fully connected layer—was used to compute SSL losses. For ARPL [12], we used a single prototype per class, a margin loss weight of 10.0, and a fixed margin radius of 1.0. For VICReg [4], SSL loss weights for similarity, standard deviation, and covariance were set to $(25.0, 25.0, 1.0)$, following the original implementation.

A.3.1. Loss Coefficients in SSL Models

The NCECE and VRCE objectives combine self-supervised and cross-entropy losses additively. To examine the effect of the self-supervised loss weight on knowledge transfer, we conducted an ablation study on $W \rightarrow N$ using the PointNet++ backbone. The cross-entropy loss weight was fixed at 1.0, while the self-supervised loss weight (SSL coefficient) was varied across $[0.01, 0.1, 1.0]$. Experimental settings, model selection, and evaluation protocols followed those described in the main paper.

The results are reported in Tab. 15 and Tab. 16. All ablated SSL models outperform supervised models in the class-split setting under LP. However, extremely small (0.01) or large (1.0) SSL coefficients reduced performance, while a moderate value (0.1) achieved the best average performance across classes. As shown in Fig. 6, a moderate SSL objective encourages class embeddings to form meaningful structures around their prototypes. In contrast, an excessively large SSL weight caused embeddings to mix

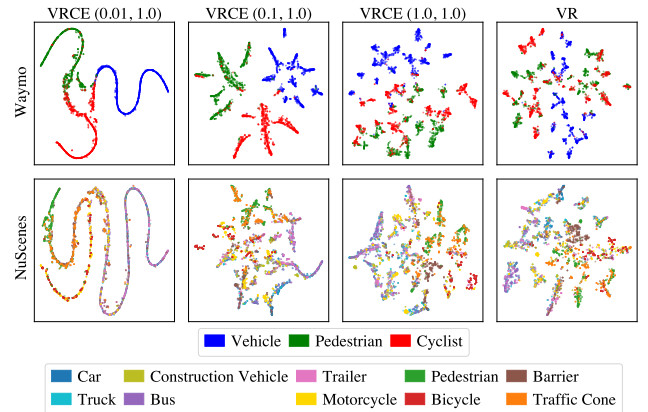


Figure 6. t-SNE plots of PointNet++ VRCE and VR base models with different loss coefficients. From left to right, the strength of SSL objective increases. The values in parentheses indicate the coefficients of the VR and CE objectives, respectively.

| Dataset | | Class Name (Number of Samples) | | | | |
|------------|-------|--------------------------------------------------------------------------------------------------------------------------------------------------------------------------------------------------------------------------------|--------------------------------------------------------|---------------------|-----------------------------------------------------------------------------------------------------------------------------------------------------------|---|
| WAYMO | Train | vehicle(647,571) | | pedestrian(367,319) | cyclist(23,542) | - |
| | Val | vehicle(161,447) | | pedestrian(87,286) | cyclist(5,910) | - |
| NuScenes | Train | car(65,025), truck(16,543), bus(4,016), trailer(5,966), construction_vehicle(2,646), motorcycle(1,128) | pedestrian(5,117) | bicycle(433) | barrier(18,917), traffic_cone(1,579) | |
| | Val | car(12,205), truck(3,351), bus(1,031), trailer(1,015), construction_vehicle(378), motorcycle(220) | pedestrian(1,139) | bicycle(57) | barrier(3,537), traffic_cone(219) | |
| ARGOVERSE2 | Train | regular_vehicle(1,354,539), bus(47,353), large_vehicle(45,511), box_truck(42,816), truck(31,458), vehicular_trailer(19,485), motorcycle(8,937), truck_cab(8,717), school_bus(6,276), articulated_bus(5,710), motorcyclist(388) | pedestrian(280,053), wheeled_rider(682), stroller(558) | cyclist(3,967) | stop_sign(32,852), sign(20,481), bicycle(15,301), construction_barrel(9,038), wheeled_device(5,249), bollard(3,592), mobile_pedestrian_crossing_sign(329) | |
| | Val | regular_vehicle(282,696), bus(7,229), large_vehicle(7,759), box_truck(9,716), truck(5,970), vehicular_trailer(5,974), motorcycle(1,724), truck_cab(4,241), school_bus(1,391), articulated_bus(996), motorcyclist(83) | pedestrian(47,634), wheeled_rider(60), stroller(72) | cyclist(323) | stop_sign(6,263), sign(3,982), bicycle(2,412), construction_barrel(2,899), wheeled_device(1,139), bollard(612), mobile_pedestrian_crossing_sign(65) | |

Table 9. Number of Train/Val samples in Waymo, NuScenes, and Argoverse2 datasets.

across classes, while an overly small weight failed to prevent neural collapse driven by the CE loss.

The SSL coefficient of 0.1, which we adopt as the default in the main paper, yielded the best performance in both CL settings in terms of ACC. Nevertheless, SSL models still do not surpass supervised ones under CL.

B. Embedding Space Visualization

In Fig. 8, we visualize the penultimate feature space of base models using t-SNE with source and target samples. The implementation is based on Scikit-Learn [42], with perplexity set to 50 and other hyperparameters kept at their default values.

In the base models, the feature space varies substantially depending on the training objective, which—as discussed in

Section 3.2.2—leads to large performance differences in LP under class-split and insertion cases. However, as illustrated in Fig. 7, such differences largely disappear after CL. This observation aligns with our findings that SSL models do not outperform supervised ones, and that the impact of the base objective becomes less pronounced in more flexible knowledge transfer settings.

C. Continual Learning with Memory: LwF with Extra-Memory

In the main paper, we assumed that no external dataset beyond the target was available during CL training. However, if a small amount of data from the old task (i.e., the source dataset) can be retained, it may substantially reduce catastrophic forgetting [31, 33, 49], leading to higher BWT and ACC. In this section, we evaluated the W→N LwF setting with additional memory across different base objectives, using a fixed PointNet++ backbone. The cross-entropy loss for the source head (before head extension) was computed on both the source memory and target training samples and distilled from the base (teacher) to CL (student) model. We employed a random buffer of 3,000 samples (1,000 per class $\in \mathcal{C}_S$) and report average accuracy over five seeds.

As shown in Tab. 10, except for the DR model, all objectives benefit from memory, with positive gains in BWT. CE, SupCon, NCE, and NCECE models also achieve ACC improvements. Notably, the NCECE model exhibits the largest gains from memory, highlighting its effectiveness when source data is available.

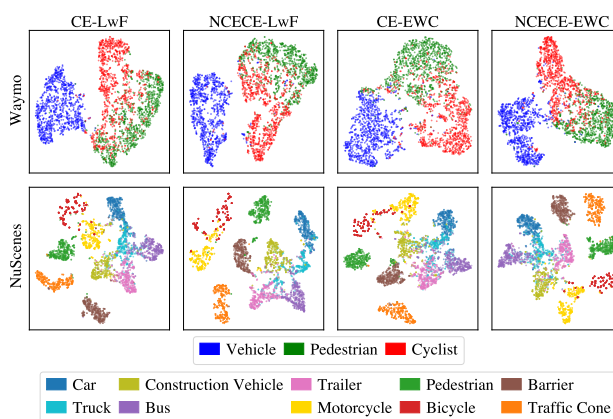


Figure 7. t-SNE plots of PointNet++ CE and NCECE W→N CL models. Column 1-2 show LwF models, and Column 3-4 show EWC models.

| W→N LwF w/ Memory | ACC | BWT | ΔACC | ΔBWT |
|------------------------------|------------------------------|------------------------------|-------------|--------------|
| CE | 88.7 (± 1.0) | -2.1 (± 1.0) | +6.2 | +14.7 |
| DR | 61.3 (± 1.2) | -58.3 (± 1.2) | -9.0 | -14.0 |
| ARPL | 85.4 (± 2.6) | -3.8 (± 2.6) | -1.5 | +5.4 |
| SupCon | 88.2 (± 0.5) | -2.9 (± 1.8) | +1.8 | +6.6 |
| NCE | 88.4 (± 2.7) | -0.1 (± 0.7) | +6.0 | +12.4 |
| NCECE | 90.6 (± 0.5) | -3.0 (± 0.6) | +6.6 | +15.6 |
| VR | 84.3 (± 1.9) | -3.0 (± 2.7) | -0.2 | +2.3 |
| VRCE | 89.1 (± 0.9) | -2.7 (± 1.2) | -8.1 | +7.3 |

Table 10. ACC(%) and BWT(%) of Waymo-to-NuScenes LwF continual learning models with additional memory for Waymo. Values in parentheses denote the standard deviation across five random seeds. Δ ACC and Δ BWT represent the performance gains compared to models without additional memory.

D. Knowledge Transfer without Domain Shift: NuScenes-to-NuScenes

In the main body, we jointly considered domain and label shifts, which is a more realistic scenario. Here, we instead isolate the case of label shift only by evaluating knowledge transfer tasks within the same dataset. Specifically, we reconstructed the NuScenes dataset into a 3-class source set consisting of `vehicle`, `pedestrian`, and `bicycle`. The `vehicle` class aggregates `car`, `truck`, `construction-vehicle`, `bus`, `trailer`, and `motorcycle`. We refer to this reconstructed set as the NuScenes 3-class dataset (N3), and denote transfer from N3 to the original 10-class NuScenes dataset as N3→N. Since both the source and target datasets were drawn from the same domain, we excluded the zero-shot transfer (which would trivially evaluate the same dataset twice) and class expansion case.

We trained 20 epochs for base models; 10 epochs for SupCon, NCE, and VR models' last-layer fine-tuning; 10 epochs for LP; and 20 epochs for CL. The learning rate was set to 10^{-3} for all models, except for ARPL base training, which used 10^{-4} due to representation collapse observed at 10^{-3} . All other settings followed those in the main paper.

In Tab. 17 and Tab. 18, we report results under the LP and CL settings, respectively. Unlike the W→N case, SSL models tend to underperform compared to supervised models on the source dataset. In addition, in the LP setting,

they achieved comparable performance in the class-split scenario, but for the maintained classes, NCE and VR models even performed worse, while showing relatively higher performance on the inserted classes. This suggests a trade-off and implies that, whereas SSL objectives contributed to transferable representations in W→N, they failed to do so in N3→N. One possible explanation is that NuScenes provides far fewer training samples (about 1/10 of Waymo), which may limit the effectiveness of SSL-based representation learning.

In the CL setting, results are largely consistent with W→N: (1) LwF consistently outperforms EWC, (2) SSL models are not superior to supervised ones, and (3) the DR model still underperforms under LwF. A key difference, however, is the presence of positive BWT. This can be attributed to fine-tuning on the same dataset, which allows the model to acquire more knowledge of the domain and thus improve classification. Moreover, since CL here involves refining coarse categories into finer-grained ones, the process may help retain or even enhance the ability to discriminate broader categories (e.g., `vehicle`) established during the base session. Such positive BWT is particularly evident in SSL models, suggesting that although their base performance was weaker, CL fine-tuning enables them to close the gap with supervised models. As shown in the last column of Tab. 18, SSL models notably improve their performance on the `vehicle` class after CL.

E. Additional Tables

The performance of best-performing CL models of Section 3.2.3 are shown in Tab. 11, Tab. 12, Tab. 13, and Tab. 14. Cells are color-coded for clarity, with brighter colors indicating higher accuracy, and bold values denoting the best performance.

| W→N LwF | ACC | BWT | NuScenes | | | | Waymo | | |
|-------------------|--------|-------------|-------------|-------------|-------------|-------------|-------------|-------------|-------------|
| | | | Veh.S. | Ped.M. | Cyc.E. | Insert. | Veh. | Ped. | Cyc. |
| PointNet++ | CE | 82.5 | -16.8 | 82.7 | 79.0 | 94.7 | 96.1 | 99.4 | 98.7 |
| | DR | 70.3 | -44.3 | 82.5 | 90.5 | 89.5 | 98.6 | 27.0 | 97.8 |
| | ARPL | 86.9 | -9.2 | 82.7 | 91.8 | 93.0 | 98.9 | 97.8 | 84.4 |
| | SupCon | 86.4 | -9.5 | 80.5 | 94.0 | 94.7 | 97.2 | 99.0 | 91.2 |
| | NCE | 82.4 | -12.5 | 78.4 | 92.8 | 82.5 | 99.2 | 99.0 | 78.2 |
| | NCECE | 84.0 | -18.6 | 83.3 | 94.0 | 96.5 | 98.5 | 99.5 | 96.5 |
| | VR | 84.5 | -5.3 | 81.3 | 98.9 | 89.5 | 96.3 | 90.2 | 74.7 |
| Point Transformer | VRCE | 87.2 | -10.0 | 81.7 | 95.6 | 91.2 | 98.6 | 99.5 | 93.6 |
| | CE | 89.2 | -4.6 | 80.5 | 90.6 | 96.5 | 97.7 | 97.3 | 96.7 |
| | DR | 70.8 | -36.0 | 80.2 | 93.6 | 91.2 | 96.8 | 2.9 | 88.6 |
| | ARPL | 84.9 | -11.3 | 79.6 | 93.4 | 93.0 | 97.0 | 93.8 | 88.8 |
| | SupCon | 87.2 | -6.6 | 78.4 | 93.7 | 96.5 | 95.6 | 96.1 | 95.7 |
| | NCE | 87.7 | -3.0 | 80.9 | 87.1 | 96.5 | 97.9 | 99.1 | 76.5 |
| | NCECE | 87.4 | -6.4 | 78.2 | 89.3 | 98.3 | 97.4 | 98.1 | 95.4 |
| Point Transformer | VR | 85.3 | -3.3 | 80.0 | 89.8 | 93.0 | 98.7 | 95.6 | 92.6 |
| | VRCE | 86.0 | -7.8 | 79.1 | 91.3 | 87.7 | 96.5 | 97.8 | 97.4 |

Table 11. Accuracies(%) of Waymo-to-NuScenes LwF continual learning models. Best λ 's are selected by ACC for each base model.

| W→N EWC | ACC | BWT | NuScenes | | | | Waymo | | |
|-------------------|--------|-------------|--------------|-------------|-------------|-------------|-------------|-------------|-------------|
| | | | Veh.S. | Ped.M. | Cyc.E. | Insert. | Veh. | Ped. | Cyc. |
| PointNet++ | CE | 74.8 | -29.7 | 76.8 | 96.3 | 84.2 | 97.7 | 47.9 | 95.7 |
| | DR | 79.5 | -25.7 | 80.6 | 96.1 | 93.0 | 98.1 | 66.0 | 74.7 |
| | ARPL | 75.8 | -30.7 | 81.4 | 96.6 | 93.0 | 97.5 | 65.0 | 78.0 |
| | SupCon | 73.4 | -30.4 | 72.8 | 85.5 | 96.5 | 98.5 | 49.3 | 69.5 |
| | NCE | 73.4 | -32.4 | 81.0 | 96.8 | 84.2 | 97.8 | 76.1 | 76.2 |
| | NCECE | 80.7 | -20.3 | 74.9 | 93.4 | 98.3 | 98.5 | 69.2 | 82.6 |
| | VR | 71.0 | -30.8 | 78.3 | 95.7 | 91.2 | 97.9 | 67.2 | 76.2 |
| Point Transformer | VRCE | 80.1 | -17.6 | 71.7 | 92.9 | 96.5 | 94.6 | 63.6 | 84.5 |
| | CE | 80.5 | -18.6 | 81.6 | 80.8 | 80.7 | 90.4 | 86.3 | 69.5 |
| | DR | 79.5 | -16.8 | 79.2 | 89.7 | 82.5 | 96.7 | 75.1 | 79.1 |
| | ARPL | 67.7 | -30.3 | 68.1 | 88.8 | 26.3 | 91.0 | 76.3 | 91.5 |
| | SupCon | 77.5 | -21.5 | 74.6 | 89.9 | 77.2 | 95.7 | 72.0 | 81.2 |
| | NCE | 75.9 | -23.8 | 76.1 | 95.7 | 93.0 | 95.4 | 73.6 | 89.0 |
| | NCECE | 76.3 | -27.8 | 77.9 | 88.5 | 91.2 | 97.3 | 72.7 | 65.6 |
| Point Transformer | VR | 73.2 | -24.1 | 77.8 | 89.5 | 77.2 | 95.7 | 63.4 | 67.7 |
| | VRCE | 73.9 | -24.9 | 67.7 | 92.8 | 87.7 | 94.6 | 65.8 | 71.4 |
| | | | | | | | | | 73.7 |

Table 12. Accuracies(%) of Waymo-to-NuScenes EWC continual learning models. Best λ 's are selected by ACC for each base model.

| W→A LwF | ACC | BWT | Argoverse2 | | | | | Waymo | | | |
|-------------------|--------|-------------|-------------|-------------|-------------|--------------|-------------|-------------|-------------|-------------|-------------|
| | | | Veh.S. | Ped.S. | Ped.SE. | Cyc.M. | Insert. | Veh. | Ped. | Cyc. | |
| PointNet++ | CE | 73.6 | -12.5 | 53.8 | 66.8 | 67.6 | 69.5 | 78.4 | 99.9 | 87.6 | 61.5 |
| | DR | 71.7 | -19.7 | 56.0 | 65.2 | 83.1 | 64.5 | 77.3 | 71.1 | 91.3 | 71.9 |
| | ARPL | 78.3 | -4.2 | 54.9 | 78.4 | 97.2 | 38.0 | 78.4 | 98.5 | 80.3 | 93.9 |
| | SupCon | 75.5 | -5.4 | 49.6 | 61.3 | 85.9 | 63.9 | 73.4 | 99.2 | 96.5 | 75.5 |
| | NCE | 69.9 | -19.1 | 55.0 | 79.1 | 62.0 | 55.1 | 81.4 | 99.8 | 94.8 | 27.0 |
| | NCECE | 73.4 | -18.7 | 54.9 | 80.3 | 97.2 | 53.0 | 81.9 | 99.5 | 99.2 | 38.8 |
| | VR | 76.0 | -2.6 | 55.5 | 69.2 | 100.0 | 67.9 | 80.2 | 98.7 | 79.4 | 76.5 |
| | VRCE | 78.2 | -5.5 | 58.4 | 71.2 | 93.0 | 27.7 | 74.8 | 99.8 | 95.6 | 78.8 |
| Point Transformer | CE | 74.1 | -9.0 | 49.2 | 44.8 | 91.6 | 81.9 | 75.5 | 99.3 | 98.7 | 64.7 |
| | DR | 71.4 | -12.1 | 57.6 | 60.2 | 26.8 | 74.1 | 76.6 | 85.6 | 96.2 | 57.0 |
| | ARPL | 66.8 | -29.8 | 58.7 | 81.5 | 95.8 | 55.4 | 77.0 | 97.6 | 98.6 | 0.0 |
| | SupCon | 74.5 | -8.0 | 51.9 | 54.2 | 94.4 | 62.3 | 70.7 | 98.3 | 93.5 | 73.8 |
| | NCE | 74.3 | -4.7 | 50.8 | 41.4 | 97.2 | 73.8 | 76.6 | 97.6 | 85.7 | 78.4 |
| | NCECE | 75.4 | -7.6 | 56.8 | 37.1 | 91.6 | 67.0 | 73.3 | 99.6 | 81.6 | 84.5 |
| | VR | 74.6 | -1.8 | 52.2 | 44.7 | 90.1 | 83.5 | 78.2 | 98.9 | 89.4 | 70.2 |
| | VRCE | 70.7 | -11.9 | 50.5 | 56.2 | 40.9 | 48.6 | 74.5 | 99.1 | 99.2 | 51.7 |

Table 13. Accuracies(%) of Waymo-to-Argoverse2 LwF continual learning models. Best λ 's are selected by ACC for each base model.

| W→A EWC | ACC | BWT | Argoverse2 | | | | | Waymo | | | |
|-------------------|--------|-------------|--------------|-------------|-------------|--------------|-------------|-------------|-------------|-------------|--------------|
| | | | Veh.S. | Ped.S. | Ped.SE. | Cyc.M. | Insert. | Veh. | Ped. | Cyc. | |
| PointNet++ | CE | 52.7 | -53.8 | 51.1 | 70.2 | 66.2 | 48.9 | 83.2 | 17.0 | 39.7 | 68.6 |
| | DR | 57.5 | -44.2 | 50.3 | 66.3 | 64.8 | 45.2 | 79.3 | 67.4 | 93.3 | 0.0 |
| | ARPL | 39.6 | -80.1 | 51.8 | 61.9 | 85.9 | 81.0 | 79.0 | 17.0 | 1.1 | 26.9 |
| | SupCon | 50.5 | -52.0 | 46.0 | 54.6 | 90.1 | 50.8 | 71.6 | 82.4 | 48.9 | 0.0 |
| | NCE | 61.8 | -30.6 | 47.2 | 89.7 | 100.0 | 18.7 | 75.5 | 98.7 | 88.4 | 0.0 |
| | NCECE | 57.2 | -42.0 | 52.2 | 59.6 | 84.5 | 22.1 | 69.6 | 71.0 | 95.1 | 1.4 |
| | VR | 48.7 | -54.8 | 52.5 | 81.8 | 84.5 | 40.8 | 79.8 | 0.0 | 97.2 | 0.6 |
| | VRCE | 40.2 | -76.9 | 48.2 | 62.4 | 84.5 | 67.0 | 74.9 | 49.2 | 0.3 | 10.3 |
| Point Transformer | CE | 51.1 | -54.6 | 48.1 | 56.3 | 95.8 | 50.2 | 76.7 | 41.3 | 13.4 | 71.2 |
| | DR | 44.9 | -58.4 | 43.8 | 51.9 | 80.3 | 67.9 | 72.6 | 0.0 | 0.0 | 100.0 |
| | ARPL | 48.2 | -62.3 | 56.5 | 73.6 | 87.3 | 27.7 | 73.5 | 2.4 | 15.5 | 80.9 |
| | SupCon | 38.7 | -74.7 | 45.7 | 40.0 | 69.0 | 65.7 | 72.0 | 47.1 | 18.5 | 0.1 |
| | NCE | 44.8 | -60.3 | 51.6 | 46.8 | 32.4 | 75.7 | 72.3 | 93.7 | 1.1 | 0.0 |
| | NCECE | 41.4 | -69.7 | 49.0 | 55.1 | 29.6 | 60.1 | 71.5 | 56.1 | 1.4 | 22.0 |
| | VR | 44.5 | -54.1 | 45.0 | 51.4 | 71.8 | 62.6 | 69.0 | 0.3 | 99.4 | 1.7 |
| | VRCE | 45.2 | -65.5 | 53.0 | 75.9 | 73.2 | 12.2 | 73.8 | 49.2 | 29.5 | 10.3 |

Table 14. Accuracies(%) of Waymo-to-Argoverse2 EWC continual learning models. Best λ 's are selected by ACC for each base model.

| Coef. | Waymo | | | W→N (Zero-Shot) | | | W→N (Linear Probe) | | | | |
|-------|-------------|-------------|-------------|-----------------|-------------|-------------|--------------------|-------------|-------------|-------------|-------------|
| | Veh. | Ped. | Cyc. | Veh.S. | Ped.M. | Cyc.E. | Veh.S. | Ped.M. | Cyc.E. | Insert. | |
| NCECE | 0.01 | 99.7 | 98.9 | 94.5 | 97.2 | 90.4 | 56.1 | 37.0 | 75.2 | 71.9 | 68.4 |
| | 0.1 | 99.5 | 98.8 | 95.3 | 96.3 | 95.3 | 59.7 | 44.6 | 82.6 | 84.2 | 70.7 |
| | 1.0 | 99.5 | 98.5 | 95.0 | 95.5 | 86.1 | 71.9 | 43.1 | 80.1 | 80.7 | 79.4 |
| VRCE | 0.01 | 99.4 | 98.1 | 96.9 | 92.6 | 90.7 | 49.1 | 32.2 | 92.2 | 42.1 | 17.0 |
| | 0.1 | 99.7 | 97.0 | 94.0 | 96.5 | 82.1 | 52.6 | 32.3 | 52.5 | 80.7 | 57.1 |
| | 1.0 | 96.5 | 94.1 | 88.0 | 97.2 | 79.3 | 47.4 | 29.3 | 77.8 | 57.9 | 63.6 |

Table 15. Accuracy(%) of PointNet++ NCECE and VRCE models with varying loss coefficients, evaluated on the validation sets of Waymo and NuScenes under zero-shot and linear probe settings. Coef. denotes the weight of the self-supervised objective.

| W→N LwF | Coef. | ACC | BWT | NuScenes | | | | Waymo | | |
|---------|-------------|-------------|--------------|-------------|-------------|-------------|-------------|-------------|-------------|-------------|
| | | | | Veh.S. | Ped.M. | Cyc.E. | Insert. | Veh. | Ped. | Cyc. |
| NCECE | 0.01 | 80.0 | -23.6 | 79.4 | 91.0 | 94.7 | 98.5 | 98.1 | 98.0 | 26.1 |
| | 0.1 | 84.0 | -18.6 | 83.3 | 94.0 | 96.5 | 98.5 | 99.5 | 96.5 | 41.9 |
| | 1.0 | 80.3 | -21.9 | 76.1 | 95.8 | 98.3 | 98.2 | 97.3 | 98.8 | 31.4 |
| VRCE | 0.01 | 77.7 | -27.7 | 79.0 | 95.4 | 82.5 | 98.8 | 97.5 | 99.6 | 14.3 |
| | 0.1 | 87.2 | -10.0 | 81.7 | 95.6 | 91.2 | 98.6 | 99.5 | 93.6 | 67.5 |
| | 1.0 | 82.0 | -15.5 | 79.5 | 99.1 | 94.7 | 97.9 | 91.9 | 93.5 | 46.6 |

W→N EWC

| W→N EWC | Coef. | ACC | BWT | NuScenes | | | | Waymo | | |
|---------|-------------|-------------|--------------|-------------|-------------|-------------|-------------|-------------|-------------|-------------|
| | | | | Veh.S. | Ped.M. | Cyc.E. | Insert. | Veh. | Ped. | Cyc. |
| NCECE | 0.01 | 75.4 | -33.1 | 78.8 | 96.0 | 98.3 | 98.4 | 50.5 | 75.5 | 67.6 |
| | 0.1 | 80.7 | -20.3 | 74.9 | 93.4 | 98.3 | 98.5 | 69.2 | 82.6 | 80.9 |
| | 1.0 | 79.9 | -22.6 | 78.1 | 93.9 | 94.7 | 94.9 | 81.3 | 84.6 | 59.4 |
| VRCE | 0.01 | 80.0 | -24.9 | 82.0 | 95.0 | 84.2 | 98.0 | 70.0 | 84.8 | 65.0 |
| | 0.1 | 80.1 | -17.6 | 71.7 | 92.9 | 96.5 | 94.6 | 63.6 | 84.5 | 89.8 |
| | 1.0 | 72.8 | -33.1 | 79.1 | 96.8 | 89.5 | 98.6 | 65.0 | 80.0 | 34.3 |

Table 16. Accuracy(%) of PointNet++ NCECE and VRCE models with varying loss coefficients, evaluated on the validation sets of Waymo and NuScenes under LwF and EWC continual learning settings. Coef. denotes the weight of the self-supervised objective. Best λ 's are selected by ACC for each base model.

| | NuScenes 3-Class (N3) | | | N3→N (Linear Probe) | | | |
|--------|-----------------------|-------------|-------------|---------------------|-------------|-------------|-------------|
| | Veh. | Ped. | Cyc. | Veh.S. | Ped.M. | Cyc.M. | Insert. |
| CE | 98.3 | 99.1 | 89.5 | 22.7 | 93.5 | 87.7 | 12.3 |
| DR | 95.5 | 99.0 | 94.7 | 22.4 | 83.4 | 94.7 | 25.2 |
| ARPL | 97.1 | 97.3 | 78.9 | 23.1 | 90.1 | 63.2 | 33.0 |
| SupCon | 98.5 | 99.5 | 94.7 | 26.5 | 76.1 | 77.2 | 31.9 |
| NCE | 79.7 | 86.7 | 73.7 | 27.2 | 55.1 | 56.1 | 59.6 |
| NCECE | 98.8 | 98.5 | 52.6 | 23.8 | 87.4 | 71.9 | 25.5 |
| VR | 87.5 | 89.9 | 84.2 | 25.3 | 66.4 | 24.6 | 53.8 |
| VRCE | 99.1 | 96.1 | 29.8 | 22.7 | 89.5 | 56.1 | 28.0 |

Table 17. Accuracy(%) of PointNet++ models on the NuScenes 3-class-to-NuScenes task under validation and linear probing settings.

| N3→N LwF | ACC | BWT | Nusscenes | | | | NuScenes 3-Class (N3) |
|----------|-------------|--------------|-------------|-------------|-------------|-------------|-----------------------|
| | | | Veh.S. | Ped.M. | Cyc.M. | Insert. | |
| CE | 90.1 | -1.3 | 79.8 | 94.5 | 89.5 | 98.2 | 99.2 |
| DR | 86.6 | -8.4 | 79.0 | 91.2 | 91.2 | 98.0 | 81.4 |
| ARPL | 93.3 | +7.1 | 81.8 | 96.8 | 98.3 | 98.7 | 99.5 |
| SupCon | 91.5 | -1.6 | 80.4 | 95.4 | 93.0 | 99.0 | 99.5 |
| NCE | 91.5 | +15.3 | 81.9 | 95.4 | 93.0 | 98.4 | 97.4 |
| NCECE | 91.3 | +13.5 | 78.6 | 95.9 | 94.7 | 97.8 | 99.7 |
| VR | 91.0 | +6.7 | 82.4 | 96.6 | 92.8 | 98.4 | 92.2 |
| VRCE | 90.0 | +19.1 | 79.9 | 84.5 | 98.3 | 98.6 | 99.7 |

| N3→N EWC | | | | | | | |
|----------|-------------|--------------|-------------|-------------|--------------|-------------|-------------|
| CE | 86.2 | -0.7 | 64.8 | 95.3 | 92.9 | 99.0 | 96.7 |
| DR | 89.9 | 0.0 | 74.7 | 94.9 | 96.4 | 98.3 | 97.8 |
| ARPL | 92.6 | +6.4 | 81.7 | 92.6 | 100.0 | 97.7 | 99.8 |
| SupCon | 89.7 | -3.1 | 77.6 | 92.1 | 92.9 | 99.5 | 98.6 |
| NCE | 90.9 | +15.1 | 81.0 | 96.5 | 89.3 | 97.9 | 99.5 |
| NCECE | 80.9 | +8.6 | 56.2 | 88.6 | 89.3 | 91.9 | 97.7 |
| VR | 90.0 | +10.3 | 73.9 | 97.0 | 96.4 | 94.5 | 99.0 |
| VRCE | 74.1 | +8.4 | 52.1 | 84.0 | 67.9 | 91.6 | 98.4 |

Table 18. Accuracy(%) of PointNet++ models on the NuScenes 3-class-to-NuScenes task under LwF and EWC continual learning settings. Best λ 's are selected by ACC for each base model.

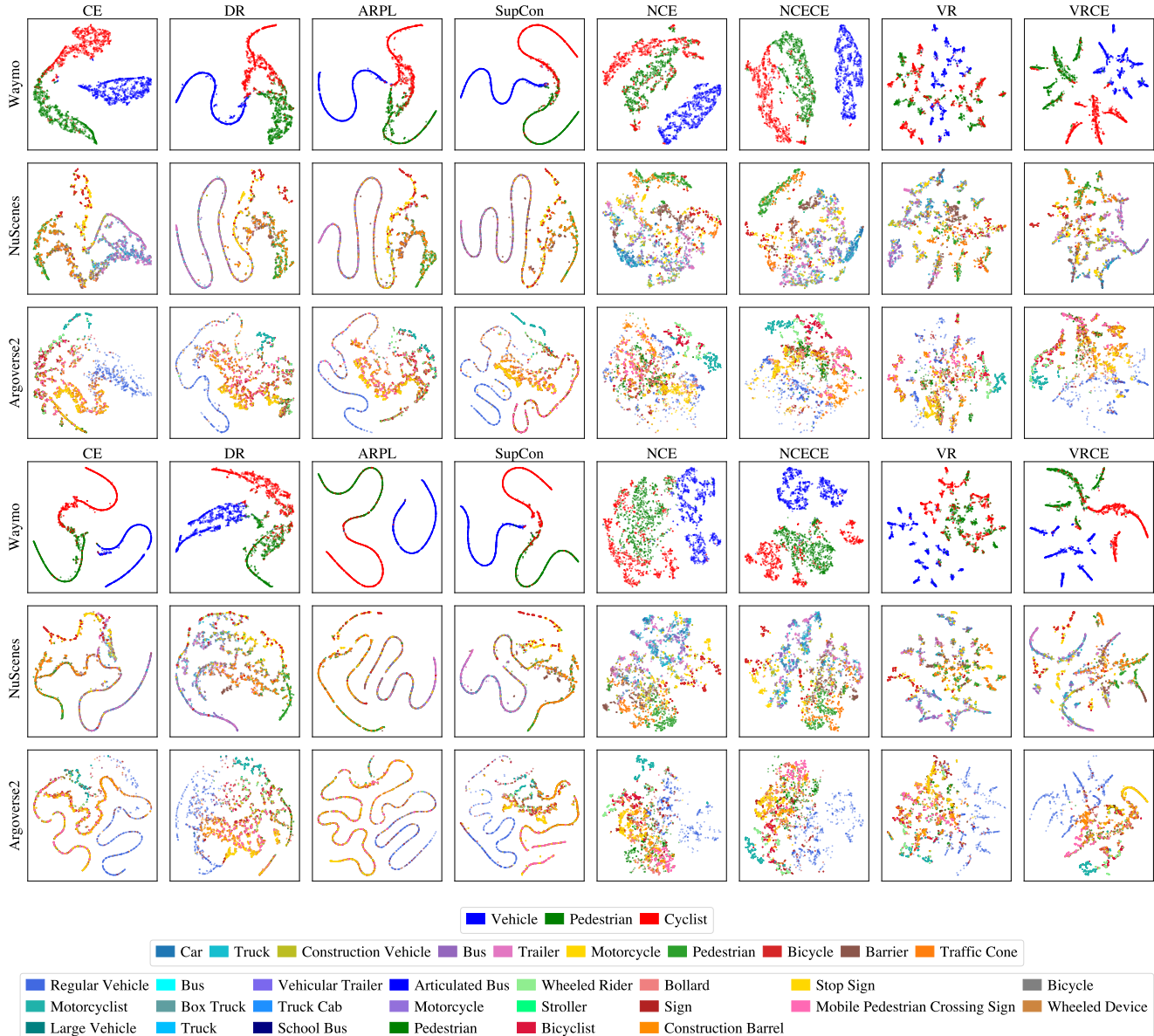


Figure 8. t-SNE plots of base models: Rows 1–3 show PointNet++ backbones, and Rows 4–6 show Point Transformer backbones.